# Dynamic rupture scenarios of anticipated Nankai-Tonankai earthquakes, southwest Japan

Sébastien Hok, Eiichi Fukuyama, Chihiro Hashimoto

# Dynamic rupture scenarios of anticipated Nankai-Tonankai earthquakes, southwest Japan

Sébastien Hok,[1] Eiichi Fukuyama,[1] and Chihiro Hashimoto[2]

Received 28 April 2011; revised 14 October 2011; accepted 20 October 2011; published 30 December 2011.

[1] We investigated dynamic rupture scenarios of anticipated megathrust earthquakes on the Nankai-Tonankai subduction zone, southwest Japan. To improve the scenario reliability, the model parameters should be constrained by available data, or derived from their analysis. We employed the three-dimensional plate interface geometry and the slip-deficit rate on the interface. Accumulated slip-deficit was used to obtain the stress drop distribution of anticipated earthquakes. The estimated stress drop distribution is consistent with the seismogenic asperity locations known from the analysis of past earthquakes. Fault friction constitutive parameters, however, had to be assumed from indirect observations because they cannot be constrained directly by the data. Based on various geophysical observations, we defined three regions where larger fracture energy is required. These are the eastern edge of the Tonankai area, the western edge of the Nankai area, and the region between the Tonankai and Nankai areas (beneath the Kii peninsula). Such lateral heterogeneity promoted the segmented rupture along the Nankai trough. With predefined stress drop and constitutive parameters, various rupture scenarios for Tonankai and Nankai asperities were obtained for different initiation locations. In some cases, a single segment is ruptured, while in other cases, all the segments are broken due to dynamic linkage at the segment boundary, causing a giant earthquake. The initiation location is a critical parameter that controls the rupture propagation across the segment boundary. These scenarios will be extremely useful to evaluate deterministically the strong ground motions and tsunami hazards caused by the next major earthquakes in southwest Japan.

**Citation:** Hok, S., E. Fukuyama, and C. Hashimoto (2011), Dynamic rupture scenarios of anticipated Nankai-Tonankai earthquakes, southwest Japan, *J. Geophys. Res.*, *116*, B12319, doi:10.1029/2011JB008492.

## 1. Introduction

[2] The Nankai trough, located in southwest Japan, is one of the most investigated subduction zones. Large earthquakes ($M_w$ > 8) occurred every 100 to 200 years [e.g., *Rydelek and Sacks*, 2003; *Ishibashi*, 2004] as a consequence of the oblique subduction of the Philippine Sea plate beneath Japanese islands at a rate of 4–6 cm/yr toward the west-northwest [*Seno et al.*, 1993; *Miyazaki and Heki*, 2001]. Nankai subduction zone is about 600 km long from its northeastern edge near the Tokai area to its southwestern edge between west of Shikoku and east of Kyushu islands (Figure 1).

[3] In this region, human societies have been developing since the sixth century and many historical documents regarding earthquakes are available, resulting in one of the longest historical records in the world. In addition, tsunami deposits have been investigated and dated precisely [e.g., *Komatsubara and Fujiwara*, 2007]. Based on these historical records, several major subduction earthquakes have been identified, and the seismic cycle in this region was investigated. It was found that all large earthquakes in the past occurred periodically [e.g., *Usami*, 1987; *Sugiyama*, 1994; *Kumagai*, 1996; *Rydelek and Sacks*, 2003; *Ishibashi*, 2004]. The most recent event occurred in 1944 (Tonankai earthquake, M 7.9) and 1946 (Nankai earthquake, M 8.0). As a consequence, large earthquakes are expected again in the following decades.

[4] From the historical records, the ruptured areas of the past earthquakes have been estimated. Based on the distribution of slip regions of large earthquakes and geomorphological considerations, two main segments have been identified along the seismogenic zone [e.g., *Ando*, 1975], one on each side of the Kii peninsula (Figure 1). The two segments broke either simultaneously or separately with relatively short separation time (from a few hours to two years), appearing as a cascaded rupture.

[5] The latest event (1944–1946) was a segmented rupture. This is the only earthquake sequence for which some instrumentally observed data were available. The 1944 Tonankai and the 1946 Nankai earthquakes occurred successively, rupturing most of the Nankai subduction zone, except at its both edges. The westernmost region, the Hyuganada area, released energy continuously by relatively small (M < 7.5) earthquakes, in 1931 (M 7.1), 1941 (M 7.2), 1961

[1]National Research Institute for Earth Science and Disaster Prevention, Tsukuba, Japan.
[2]Graduate School of Environmental Studies, Nagoya University, Nagoya, Japan.


0148-0227/11/2011JB008492

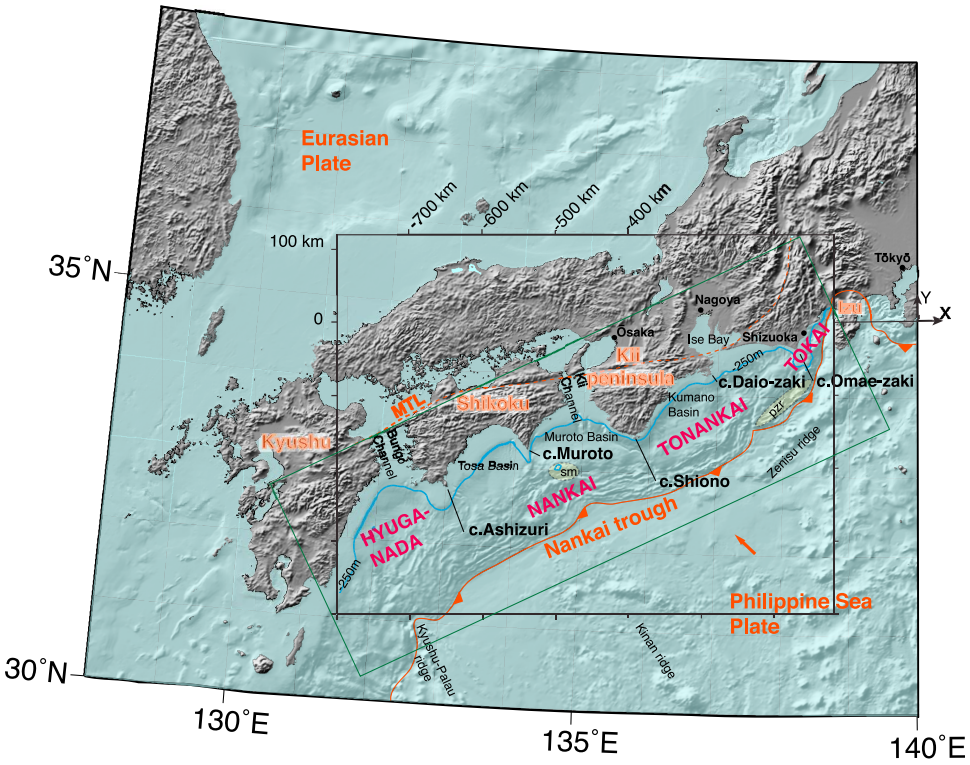


**Figure 1.** Topographic map of southwest Japan. The −250 m isodepth in the shelf bank is underlined with thick blue-gray contour. Abbreviations 'sm,' 'pzr' and 'c.' stand for subducted seamount, subducted paleo-Zenisu ridge and cape, respectively. Black rectangle shows the computation area shown in the following, and the XY coordinate system used, whose origin is located at (35°N, 140°E). Rotated green rectangle shows the area covered by free surface elements.

(M 7.0) and 1968 (M 7.5) [*Yoshioka*, 2007]. The Tokai area, the easternmost region, remained unbroken so far, which led to suspect a high-risk seismic gap close to the populated Shizuoka area [*Ishibashi*, 1981]. Both epicenters of 1940s earthquakes were located south of the Kii peninsula, the central part of the trench [*Kanamori*, 1972]. The ruptures of these earthquakes propagated mainly in opposite directions. Most inversion analyses for coseismic slip distribution indicate that the slip areas of these earthquakes overlapped each other [e.g., *Baba and Cummins*, 2005]. Therefore, one of the remaining issues to be solved is why the rupture did not propagate bilaterally to the western segment in 1944.

[6] Analyses of historical documents allow us to investigate the characteristics of the past huge earthquakes, although they should include uncertainties. The previous events of 1854 are also known as a twin event; a segmentation pattern similar to the 1944–1946 earthquake sequence was revealed by the seismic intensity distribution estimated from the historical documents. The epicenter of the first earthquake might have been located in the Tokai region (making this event larger than the 1944 earthquake). The second 1854 earthquake is suspected to have larger magnitude, possibly breaking farther west than what is considered for the 1946 Nankai earthquake [e.g., *Sugiyama*, 1994; *Furumura et al.*, 2011]. The preceding 1707 earthquake is known as a single giant event that broke the whole Nankai subduction zone at a time, breaking larger area than the 1944–1946 and 1854 events [*Furumura et al.*, 2011]. From the re-examination of historical documents, *Matsu'ura et al.* [2010] suggested that the 1707 rupture initiated in the Tokai area, propagated unilaterally, and broke the whole plate interface.

[7] From the compilation of the past earthquake source models as described above, both a segmented and a single rupture can occur and should be taken into account in the modeling. There is a particularly critical area beneath the Kii peninsula, which is located between the Nankai and Tonankai areas and separates the two main segments. It seems thus to behave as a conditional barrier to the rupture.

[8] To contribute to the mitigation of disasters from future megathrust earthquakes, construction of possible rupture scenarios should be very useful. Such rupture scenarios can then be used for strong ground motion and tsunami simulations. For instance, *Sekiguchi et al.* [2008] studied the strong ground motion in Osaka basin caused by a kinematic rupture model of the Nankai earthquake. Using a quasi-dynamic model with rate-and-state friction evolution, *Kodaira et al.* [2006] obtained spontaneous ruptures which reproduced the seismic cycle characteristics along the Nankai trough, including the segmentation. However, in addition to a quasi-dynamic assumption [e.g., *Rice*, 1993], their model parameters were subjectively set up. To make the scenarios more reliable and usable for hazard mitigation, the rupture models should be based on fully elastodynamic approaches and integrate physical parameters directly from observations. The present work aims at demonstrating the feasibility of such a framework.

[9] In this paper, we propose some scenarios for the future Nankai-Tonankai earthquakes. First, we review the past studies on the Nankai subduction zone to compile the lateral variations of observed features along the Nankai trough. Then, based on the distribution of heterogeneity, we construct a set of parameters for initial stress and constitutive relation used for the dynamic rupture. Finally, we discuss the relation between obtained rupture scenarios and assumed parameter sets.

## 2. Lateral Variations in Geophysical Data Sets

[10] Since the target of this study is to construct reasonable scenarios for the generation of large earthquakes along the Nankai trough, we have to investigate whether lateral heterogeneity along the Nankai trough is significant in the modeling or not. For that purpose, we reviewed previous studies and extracted the spatial variations of observations which might have links with the constitutive parameters in the following sections.

### 2.1. Geometry of the Plate Interface

[11] One of the possible indirect observations useful for the modeling of the constitutive parameters could be the geometry of the plate interface. A large number of techniques have been applied to image the plate interface geometry at different depths, constructing a reliable picture of its complexity.

[12] At shallow depth, topographic anomalies have been identified: a seamount from Kinan ridge is subducting off cape Muroto [*Kodaira et al.*, 2000], and a paleo-Zenisu ridge has been imaged in the eastern Tonankai segment [*Le Pichon et al.*, 1996; *Kodaira et al.*, 2003]. These two structures are located above the seismogenic zone, at 5–10 km depth, and could be responsible for preventing the shallow rupture during the last two events of 1944 and 1946 [*Kodaira et al.*, 2006]. However, the rupture continued propagating along the deeper seismogenic zone. In addition, it was reported that the subducting plate basement relief is variable [*Ike et al.*, 2008], leading to non-uniform sediment composition and thickness along the trough. However, these shallow anomalies seem difficult to relate to some heterogeneity at seismogenic depth.

[13] At seismogenic depth, dip angle changes along the trench [e.g., *Baba et al.*, 2006; *Hirose et al.*, 2008; *Shiomi et al.*, 2008; *Ohta and Ide*, 2011]. Dip angle is steeper in the eastern part than in the western part. The transition is located west of the Kii peninsula. The edges of the previous earthquake rupture areas may correspond to the places where the dip angle of the plate interface changes. For instance, the eastern edge of the 1944 Tonankai earthquake is located below Ise bay, where the slab bends, and the 1946 Nankai earthquake stopped in the western Shikoku region, where a bend of the slab interface is observed. In addition, the convergence direction is almost parallel to the dip in the eastern segment, while it is oblique in the western part. These differences might affect the coseismic rupture.

### 2.2. Plate Coupling

[14] During the interseismic period, the coupling between two plate interfaces can vary from 0% (creeping) to 100% (locking), depending on local parameters such as temperature, stress environment, and rock materials. Plate coupling is primarily a function of depth. At shallow depth in the accretionary wedge, and at deep depth (either below the Moho or the 450°C isotherm), the coupling is weak, and the deformation is mostly aseismic. In contrast, at intermediate depth (between 150°C and 350°C isotherms), seismic activity occurs [*Hyndman et al.*, 1995]. Large earthquakes are generated at these depths, therefore recognized as the seismogenic zone. The coupling becomes maximum there and the stress is accumulating during the interseismic period. Moreover, the plate coupling varies laterally, creating areas of high potential strain energy release (asperities). As a consequence of the coupling at seismogenic depth, the plates deform during the interseismic period. This deformation of the plates is measured by the analysis of GPS data, and the local coupling rate of the interface can be estimated along the plate interface.

[15] Recently, in various subduction zones, from joint analysis of coseismic slip distribution and plate interface coupling distribution, a possible correlation is reported [e.g., *Perfettini et al.*, 2010; *Moreno et al.*, 2010]. Such a correlation can be observed for the recent 2011 Tohoku-oki earthquake, northeast Japan [e.g., *Suwa et al.*, 2006; *Hashimoto et al.*, 2009a; *Loveless and Meade*, 2010; *Ozawa et al.*, 2011]. In addition, *Kaneko et al.* [2010] confirmed the correlation between highly coupled patches and seismic asperities, by numerical modeling. However, in some cases, areas where coupling was found to be high were not ruptured [e.g., *Konca et al.*, 2008].

[16] At the Nankai subduction zone, models of interseismic interface coupling, or slip-deficit rate, have been developed for years [e.g., *Savage and Thatcher*, 1992; *Le Pichon et al.*, 1998; *Mazzotti et al.*, 2000; *Miyazaki and Heki*, 2001; *Heki and Miyazaki*, 2001; *Ito and Hashimoto*, 2004; *El-Fiky and Kato*, 2006; *Tabei et al.*, 2007; *Liu et al.*, 2010; *Loveless and Meade*, 2010]. From the most simple model with uniform value over a planar fault, to the modern spatially variable rates using realistic three-dimensional surfaces, they all depict the same feature: the Nankai seismogenic zone is highly coupled over its whole length. This is also shown by the lack of seismicity of the interface [e.g., *Mogi*, 1990; *Hasegawa et al.*, 2009; *Ohta and Ide*, 2011]. The coupling of the Nankai trough can be seen through the slip-deficit rate distribution estimated by *Hashimoto et al.* [2009b] (Figure 2). The slip-deficit increases from east to west, following the plate convergence rate.

[17] From the distribution of the stress accumulation estimated from the slip-deficit rate distribution of *Hashimoto et al.* [2009b] (Figure 2), we identify four potential seismic asperities (see Figures 3e and 4b), which are defined as high stress drop areas. The westernmost asperity is located in Hyuga-nada region and is considered to have ruptured during the 1707 and possibly 1854 earthquakes [*Sugiyama*, 1994; *Furumura et al.*, 2011], but not during the 1946 Nankai earthquake. However, this area was regularly ruptured by medium sized earthquakes ($M_w$ 6.5–7.5) in the 20th century [e.g., *Yoshioka*, 2007].

[18] The largest asperity in size and magnitude is located in the eastern Shikoku area, roughly centered beneath the cape Muroto. It corresponds well with the area where the largest slip was observed during the 1946 Nankai earthquake

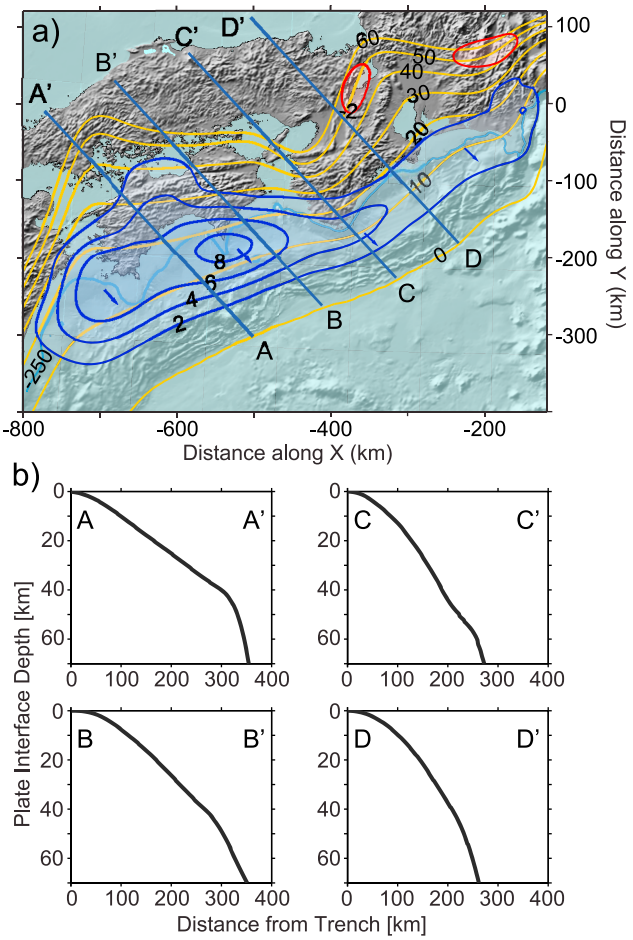


**Figure 2.** Slip-deficit rate distribution [*Hashimoto et al.*, 2009b] and three-dimensional plate geometry [*Hashimoto et al.*, 2004]. The coast line is underlined with pink contour, the −250 m isodepth with thick blue-gray. The geometry of the interface is shown by yellow contour lines every 10 km, and by four profiles taken along plate convergence direction at lines AA, BB, CC and DD, shown at the bottom. On the map, the slip-deficit rate appears in blue and red, contour lines are plotted every 2 cm/yr. The four arrows show the slip-deficit rate directions at those locations.

[e.g., *Ando*, 1975; *Tanioka and Satake*, 2001a; *Baba and Cummins*, 2005].

[19] The third asperity starts below the Kii peninsula, where the stress accumulation is slightly larger, and extends toward the east until the cape Omae-zaki. It is the longest asperity, but its accumulated stress is small. The western half of this asperity seems to match the slip location of the 1944 Tonankai earthquake [e.g., *Kikuchi et al.*, 2003; *Baba and Cummins*, 2005].

[20] Finally, the last area where the stress drop is large is the Shizuoka area. However, in our modeling, since the region was located at the edge of the computation area, the stress change could not be estimated well due to the edge effects. Therefore, we do not focus on this area in this study.

[21] We can summarize that based on the slip-deficit rate distribution, less accumulated stress zones are found east of cape Ashizuri, west of cape Shiono, and between cape Daio-zaki and cape Omae-zaki (Figure 4b).

### 2.3. Geomorphologic Bathymetry and Accretionary Prism

[22] The trench-perpendicular morphology is similar along the trough. Behind the trench, there is a steep slope (2000–3000 m high) in the frontal wedge, built by active out-of-sequence thrust faults piling. After this outer-wedge ridge, flat inner-wedge forearc basins are found. They end landward by a 2000–1000 m high steep bank, which reaches inland shelf level. This general picture has some variations, due to the decrease of trench depth from west to east, as well as the change of dip angle, discussed previously. The overall distance from the inland shelf to the trench decreases from west to east.

[23] However, there is remarkable lateral variation in the detailed structure. The shelf bank is not aligned parallel to the trench but rather wavy (Figure 1). It defines the lateral edges of inner-wedge basins. We used the 250 m depth contour line to show the location of the inland shelf slope in Figures 1, 2, and 3c. It is important to note that the bank position oscillates right above the seismogenic zone defined by the stress drop

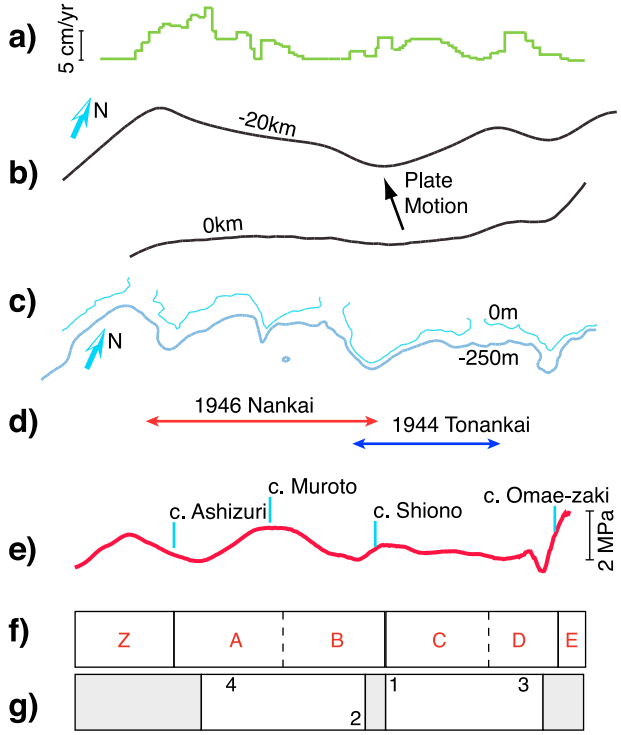


**Figure 3.** Spatial correlations between lateral variations of various parameters along the Nankai trough. (a) Tremor slip-rate profile, from *Obara* [2010]. (b) Map-view of plate interface depth contours, from *Hashimoto et al.* [2004], showing the dip angle variations. Arrow 'N' indicates north (Y axis direction). (c) Map-view of bathymetric contours. 'N' indicates north direction. (d) Extension of coseismic slip retrieved from tsunami data inversion [*Baba and Cummins*, 2005]. (e) Maximum initial stress profile derived in this study. (f) Segmentation from *Ando* [1975] and *Sugiyama* [1994]. (g) Regional segmentation for constitutive properties considered in this study. The numbers refer to initiation locations (see Figure 7).

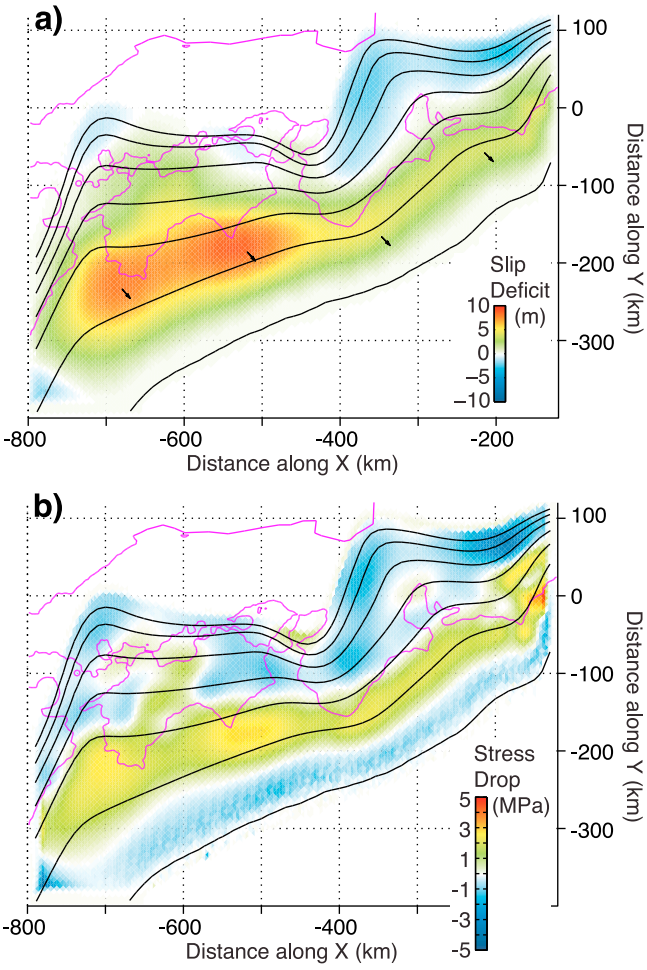


**Figure 4.** (a) Slip deficit distribution estimated for 100 years loading, assuming a constant coupling rate estimated by *Hashimoto et al.* [2009b]. Maximum value is 8.65 m. Arrows show the local slip direction. Black contours are isodepths of the plate interface [*Hashimoto et al.*, 2004], and pink contours are the coastlines. (b) Stress drop for the complete release of the slip-deficit.

distribution located between 10 km and 20 km slab-depth contours (Figure 2).

[24] It was suggested by *Sugiyama* [1994], and extrapolated for other subduction zones by *Wells et al.* [2003], that the inner-wedge basins should be considered as the surface projections of earthquake asperity locations at seismogenic depth. By identifying the bank position and its shape, we recognize three potential asperities from east to west: (1) the broader Tonankai region, delimited by the cape Omae-zaki and the Kii peninsula; (2) the Nankai source region, delimited by the Kii peninsula and the region of cape Ashizuri, which both have a similar size and shape; (3) the Hyuga-nada basin, which forms the narrowest asperity. The subdivision inside the Nankai segment by cape Muroto (Figure 1) seems to be secondary, due to the overall shape of the broad Nankai basin, and to the relatively narrow width of the cape.

[25] Reciprocally, the Kii peninsula and the southwestern part of Shikoku, which are located between the basins, are uplifted. Those uplifted areas correlate with differences in the shallow wedge structure, implying deeper under-plating [*Park et al.*, 2002; *Kimura et al.*, 2007], shallower plate interface, and larger friction. This characteristic was found in cape Ashizuri region, and explained as a possible barrier there by *Yoshioka* [2007].

[26] The morphology of the accretionary wedge could be closely related to its internal structure, as shown by analogical experiments [e.g., *Dominguez et al.*, 2000; *Rosenau and Oncken*, 2009]. Therefore, bathymetric variations along the Nankai trough could reveal some lateral variations in its internal structure. For instance, in a sandbox experiment, *Rosenau and Oncken* [2009] could observe the apparition of a basin above the wedge, according to its internal deformation style. An inner wedge basin is related to relative homogeneous elastic deformation in the wedge, whereas uplifting implies diffuse inelastic deformation inside the wedge. Therefore, we state that in Nankai subduction zone, uplifted areas may hide a more complex wedge structure than basin areas. The complexity should simply be related to active thrust faults producing under-plating processes and upward motion. This is similar to the long-term prism accretion or outer-ridge construction, but occurs above the seismogenic zone where uplift is visible. Figure 5 illustrates schematically these differences in the internal structure of the wedge. The facts that uplifted areas are rather large, spanning over a hundred of kilometers, and that there is no identified active structure close to the surface, could imply that the under-plating process and structures are deep, possibly close to the subduction interface.

[27] If structural under-plating exists at depth, the subduction interface might not be mapped to a single plane. It could be rather composed of zones with many fault branches, like those in the shallow wedge. Therefore, in these places, the megathrust rupture could be affected by the effect of significant geometrical complexity, as opposed to the simple situation of a single interface separating the slab from the overriding plate. This could be expected below the basins. Here, we hypothesize that, such geometrical complexity exists at seismogenic depth, below the Kii peninsula and cape Ashizuri region. In this way, we can link the visible morphology to the subduction interface properties. It satisfies the spatial correlation between long-term uplift and rupture propagation barrier.

### 2.4. Non-volcanic Tremors and Slow Slip Events

[28] The deep non-volcanic tremors has been observed systematically along the Nankai trough [e.g., *Obara*, 2010]. Their spatial distribution along the slab interface is not uniform. Beneath the Shikoku, Kii, and Tokai areas, *Obara* [2010] showed that the tremors occurred inside small segmented areas. We noticed that some of the boundaries can be correlated with features at seismogenic depths, although it is not clear how to relate the processes at tremor depth (30–40 km) to those in the seismogenic zone. For instance, the main gaps seem to correlate with slab bends (Figures 3a and 3b). The tremor areas and gaps might be correlated with seismogenic asperities, as there seems to be two wide patches of tremors corresponding to the Nankai and Tonankai asperities (Figures 3a and 3d). The barrier between the 1940's earthquakes correlates with the western termination of Kii peninsula's tremor patch. Below Shikoku, however, the correlation could be opposite. Highly stressed area off cape Muroto (Figure 3e) corresponds with two small segment

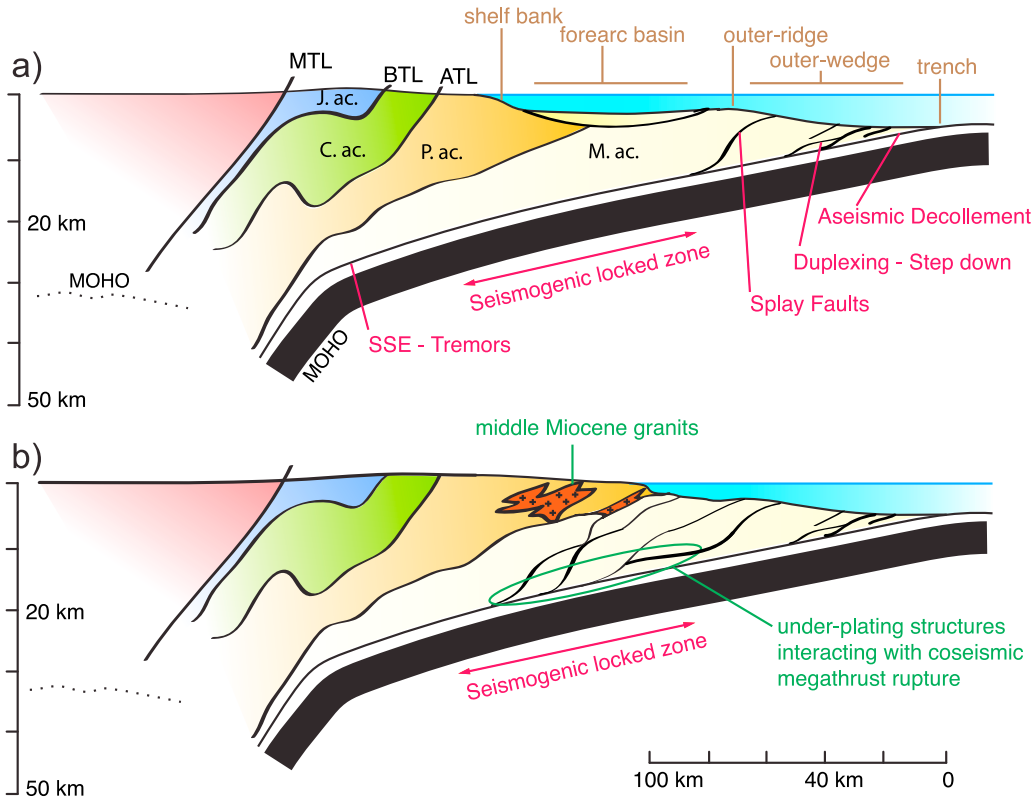


**Figure 5.** (a) Comparison of tentative internal structures in the case of a superficial basin and (b) an uplifted wedge. Inland geological structure of accretionary complex (ac) units shown in Figure 5a is simplified from *Ito et al.* [2009]. The shallow wedge structures are modified from *Kimura et al.* [2007]. 'J.,' 'C.,' 'P.,' and 'M.' stand for Jurassic, Cretaceous to early Paleogene, middle Paleogene to early Miocene, and middle Miocene to present, respectively. Metamorphic units are not shown [see *Isozaki et al.*, 2010]. 'MTL,' 'BTL,' and 'ATL' stand for Median, Butsuzo and Aki Tectonic Lines, respectively. In Figure 5b, structures circled with green are hypothetical.

of tremors at depth, while low stressed region off cape Ashizuri corresponds with the largest and most active tremor source region. In this area located in the western part of Shikoku, *Ide* [2010] suggested that some alignments in the spatial distribution of tremor sources might indicate the past convergence direction of the plates. Updip projection of these striations in the tremor zone corresponds roughly to the place where the 1946 Nankai earthquake stopped.

[29] Using the tremors as a proxy for slow-slip moment release, *Obara* [2010] calculated along-strike variation of slip release, that shows an overall agreement with slip-deficit rate in the locked zone. More slip was released in the Shikoku area than in the Kii and Tokai areas. Long-term slow slip events (SSEs) are also recorded at each edge of the Nankai trough: below the Bungo channel [*Hirose et al.*, 1999; *Hirose and Obara*, 2005], and below the Tokai area [*Ozawa et al.*, 2002]. Between 1996 and 2000, which is used for the estimation of the slip-deficit rate distribution by *Hashimoto et al.* [2009b], it should be noted that a large SSE occurred at each location. In the Hyuga-nada region, slow slip was also found to occur after the recent 1996 $M_w$ 6.8 earthquakes [e.g., *Yagi and Kikuchi*, 2003].

[30] The previous remarks indicate that the deep slow slip activity might have some connections with the slip in the seismogenic zone. However, the link is difficult to establish since underlying physical mechanisms of slow slip and tremors are still under investigation [e.g., *Ariyoshi et al.*, 2009; *Ando et al.*, 2010].

### 2.5. Geology and Bouguer Anomaly

[31] Most of the studies using gravimetric data focused on free-air anomaly [*Song and Simons*, 2003; *Llenos and McGuire*, 2007], mainly as a proxy for topography [*Wells et al.*, 2003]. However, the Bouguer anomaly reveals the wedge internal density anomalies, bringing some information closer to the slab.

[32] The upper crust of the Nankai subduction zone is composed of different accretionary complexes (located between Median Tectonic Line (MTL) and the Nankai trough in Figure 1). They were accreted by under-plating and uplifted progressively since Jurassic, when the Pacific plate was subducting in this area [e.g., *Taira*, 2001]. The upper crust internal structure is relatively homogeneous along the trench and the contacts between the different units are dipping toward north-northwest [*Ito et al.*, 2009], the youngest unit being closer from the trench [*Geological Survey of Japan*, 1992a].

[33] No lateral variation in the gravity anomaly can be found inland southwest Japan [*Geological Survey of Japan*, 1992b]. However, some strong lateral variations can be

seen offshore. An investigation of the Bouguer anomaly in the Kii peninsula area by *Honda and Kono* [2005] revealed that the density is 400 kg/m$^3$ higher in the wedge above the seimogenic zone. This anomaly is associated with the presence of granitic intrusions in the most recent accretionary unit (∼17–12 Ma [*Kimura et al.*, 2005]), due to the initiation of the Philippine Sea plate subduction below southwest Japan.

[34] When looking at the Bouguer anomaly map [*Geological Survey of Japan*, 1992b] over the whole Nankai subduction zone, we could identify other high anomaly areas around cape Ashizuri, where mafic rocks of the same age were found [*Kimura et al.*, 2005]. In contrast, low anomalies are found below Kumano, Muroto and eastern Tosa basins. At Nankai trough, although inland geology and structure are relatively homogeneous, variations in Bouguer anomaly are found offshore, above the seismogenic zone.

### 2.6. Summary of Lateral Variation Along the Nankai Subduction Zone

[35] Among the various observational data, some of them are directly related to the seismogenic zone, such as slab geometry (Figure 3b), source area of past earthquakes (Figure 3d), and stress drop distributions inferred from the slip-deficit distribution (Figure 3e). From Figures 3e and 3f, one can see a spatial correlation between the high potential stress drop areas (Hyuga-nada, off-Muroto, off-Kii peninsula and Tokai area) and known rupture segments (Z, A + B, C + D, E). In addition, each linear portion of the slab has an asperity (Figures 3b and 3e). It should be noted that the Hyuga-nada portion is truncated by the subduction of Kyushu-Palau ridge, and that the Tokai area (and eastern Tonankai) is highly influenced by the collision of Izu peninsula.

[36] Apart from these parameters directly related to the seismogenic zone, we could identify other parameters whose lateral variations are qualitatively similar. The most convincing feature is the distance between the shallow bank and the trench (Figure 3c).We can clearly recognize the western Hyuga-nada, the Nankai and the Tonankai regions as broad basins. We also notice off Kii peninsula and off cape Ashizuri as the edges of the basins. Their shapes are very similar, marked with a wide and strong seaward deflection of the bank. These two areas also corresponds to the positive Bouguer anomalies, associated with granitic intrusions which indicates possible differences in its internal structure with respect to the basin areas. This difference of structure could lead to different constitutive properties at coseismic depth.

[37] We shall take into account both direct and indirect observations reviewed above to construct the constitutive parameter distribution for the modeling of the dynamic rupture propagation, as shown in the following section.

## 3. Computation Procedure

[38] To compute the spontaneous rupture scenarios, we used a boundary integral equation method (BIEM) recently developed by *Hok and Fukuyama* [2011], which is based on the method introduced by *Fukuyama and Madariaga* [1998], *Fukuyama and Mikumo* [2006] and *Tada* [2006]. The BIEM by *Hok and Fukuyama* [2011] allows us to introduce non-planar fault interfaces with a free surface by using triangular elements. Thus, for the computation of coseismic rupture propagation, fault geometry, stress field, constitutive relation on the fault and the initiation procedure are required.

### 3.1. Fault Geometry

[39] We employed the three-dimensional geometry of the plate interface model proposed by *Hashimoto et al.* [2004], which captures the essential features of the slab complexity. The model is based on the inversion method by *Yabuki and Matsu'ura* [1992] using ISC hypocenter catalog, minimizing an ABIC that handles appropriately a priori information such as trench location and smoothness of the plate interface. The modeling was validated by comparing the long-term vertical crustal deformations with observed gravity anomalies [*Hashimoto et al.*, 2004].

[40] From this model, we built a fault interface composed of 13385 triangular elements, whose gravity centers are mapped to the 4 km interval nodes of the model of *Hashimoto et al.* [2004]. All triangle elements have a 16 km$^2$ area when they are projected to the horizontal plane; their actual size depends on the local dip angle. Figure 2 shows the slab interface geometry relatively to the coast line. The free surface is a flat rectangular area of 800 × 296 km$^2$ composed of 7400 triangular elements, each of which having a 32 km$^2$ area. The long side of the free surface directs to N65°E, the average trench direction (Figure 1).

### 3.2. Initial Stress Distribution From Slip Deficit Rate

[41] Using the same technique of *Hashimoto et al.* [2009a] for northeast Japan, *Hashimoto et al.* [2009b] estimated the slip-deficit rate distribution on the plate boundary of the Philippine Sea plate along the Nankai trough using the GEONET GPS data between 1996 and 2000 based on the 3D plate boundary model as shown previously. It gives an instantaneous picture of the coupling of the plates during 4 years in the interseismic period (Figure 2). More than 50 years passed after the previous subduction earthquakes that we believe to occur every 100–200 years along this trench. A reasonable assumption could be that the interseismic cycle is a slow but steady process that reloads progressively the plate interface between two megathrust earthquakes (see discussions in the work of *Savage* [1995]), and that the coupling ratio does not evolve significantly over the interseismic period. Then, we can reasonably extrapolate the current slip-deficit rate over a whole interseismic duration.

[42] Consequently, we made the following assumptions. (1) The great earthquakes release entirely the slip-deficit accumulated during the interseismic period. (2) During the interseismic period $T$, the cumulated slip-deficit distribution on the plate interface increases linearly, with the rate $\dot{B}(\mathbf{x})$ estimated by *Hashimoto et al.* [2009b]. The total amount of slip-deficit accumulated all over the plate before the large target earthquake is then $B(\mathbf{x}) = \dot{B}(\mathbf{x})T$. (3) The coseismic slip direction is the same as the one of the slip-deficit (i.e. plate subduction direction).

[43] In this way, we skip a full seismic cycle computation, by inferring directly the potential amount of coseismic slip from the slip-deficit rate distribution. The potential coseismic slip distribution obtained for a 100 years interseismic loading is shown in Figure 4a. It is heterogeneous and maximum at seismogenic depths. In the western half of the slab interface, the Nankai area, a substantially large slip is expected,

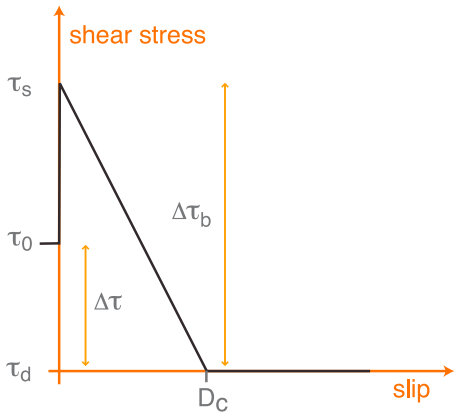


**Figure 6.** Slip-weakening constitutive law (black line) used in our dynamic rupture models, and related parameters.

spreading on a larger and deeper area along-dip, than that in the eastern half, the Tonankai area, which has higher dip angle. The estimation error of slip-deficit rates by *Hashimoto et al.* [2009b] is about 2–3 cm/yr, or 25% of the maximum value in the model. This error could be the reason why small negative values appear, or they can be the consequence of the limits of our assumption to extrapolate a slip-deficit rate over the whole cycle. As a result, this slip-deficit model cannot resolve a sharp transition at segments even if it exists.

[44] To handle properly the edge effects in the model, before the forward computation of the stress change, $\dot{B}(\mathbf{x})$ was tapered linearly to zero at the edges, between 65 and 70 km at depth (the plate interface was modeled until 70 km depth), and 10 km width at both lateral sides. There is no tapering close to the trench. After the forward computation, the stress drop is also tapered in the same way.

[45] In the first step of the modeling, we estimated the stress change distribution produced by the slip distribution which is expected from the slip-deficit distribution assumed on the plate interface. It is a kinematic modeling, in which only the slip on the interface is imposed, through a source time function. The same elastic parameters as *Hashimoto et al.* [2009b] used for the estimation of the slip-deficit rates are employed: P wave velocity ($\alpha$) is 6325 m/s, S wave velocity ($\beta$) is 3651 m/s and shear modulus ($\mu$) is $4.0 \times 10^{10}$ Pa.

[46] Using the geometry described in the previous section, we set up the time step $\Delta t$ according to a Courant-Friedrichs-Lewy condition (CFL) [*Tada and Madariaga*, 2001], ensuring that the waves generated at a given element at time $t$ do not propagate to the surrounding elements before time $t + \Delta t$. That is, $\Delta t \leq \Delta x/\alpha$, where $\Delta x$ is the shortest spatial discretization distance. Here, $\Delta x$ = 1.33 km, and the time step was set to $\Delta t$ = 0.14 s, which corresponds to 67% of the CFL condition.

[47] Using the BIEM code, we computed the evolutions of the three traction components as the sum of the contribution of the local slip and of the past slip from other subfaults through the kernels. We obtained the distribution of the static stress change for 3 traction components associated with the assumed slip distribution on the plate interface in half-space. To construct the initial stress conditions we used only the component parallel to the slip direction. The perpendicular and normal traction components were ignored because they were one order of magnitude smaller than the parallel component. It should be noted that all three traction components were taken into account to solve the dynamic rupture process of the spontaneous rupture scenarios shown later.

[48] Finally, we applied a spatial smoothing operation to the stress change distribution. Mapping a curved surface with flat elements results in elements having slightly different strike and dip angles (we assigned each triangle summit to lie on the curved surface). This fault configuration generates an oscillation in the static stress pattern. To suppress this oscillation, the computed stress drop is averaged over the three adjacent elements.

[49] Figure 4b shows the final stress drop distribution over the slab interface. It ranges from 5 MPa in asperity regions to −2 MPa in deep or shallow unlocked regions. We can see the seismogenic zone, where the stress drop is positive (meaning that there is a potential seismic energy to be released there), lying between 5 and 25 km depth in the west, and between 3 and 15 km in the east. Large lateral variations are observed inside the seismogenic zone. Four more loaded regions, that could be asperities, can be identified; (1) west of cape Ashizuri (off Bungo channel), (2) below cape Muroto, (3) east of the Kii peninsula (with a maximum below cape Shiono) and (4) below cape Omae-zaki and Shizuoka. However, as stated before, the last region could be uncertain and we do not take into account the Tokai region in this study. We will focus on the two main asperities of Tonankai and Nankai. We can also identify the three less loaded regions of east of cape Ashizuri, west of cape Shiono, and between cape Daio-zaki and cape Omae-zaki.

[50] As it has to be included in the dynamic models, the obtained stress drop distribution $\Delta\tau(\mathbf{x})$ is converted to an non-uniform initial stress distribution $\tau_0(\mathbf{x})$, while the final stress $\tau_d(\mathbf{x})$ is kept uniform. These parameters are shown in Figure 6. To avoid zero and negative shear stresses, the dynamic stress is set to

$$\tau_d(\mathbf{x}) = -1.01 \min(\Delta\tau(\mathbf{x})) \quad (1)$$

Accordingly, the initial shear stress is:

$$\tau_0(\mathbf{x}) = \Delta\tau(\mathbf{x}) - 1.01 \min(\Delta\tau(\mathbf{x})) \quad (2)$$

The maximum initial stress is about 8.5 MPa, while the dynamic friction level is close to 4.5 MPa. Initial shear stress direction is the slip-deficit direction. The initial normal stress is chosen to be uniform over the plate interface, at 40 MPa, assuming an arbitrary lithostatic pore pressure effect. The resulting initial friction coefficient is between 0.1 and 0.2 over the seismogenic zone. In the present computation, we followed *Brown et al.* [2003], who found that the shallow Nankai prism has a frictional strength lower than 0.25 at up to 40 MPa effective normal stress due to the mineral phase composition and the fluid content. In absence of other relevant information, we referred to these values for the deeper seismogenic zone.

### 3.3. Constitutive Relation

[51] Since we focus on the unstable rupture propagation, we employ a linear slip-weakening law originally proposed by *Ida* [1972] (Figure 6). The slip-weakening law requires

two critical parameters, slip-weakening distance ($D_c$) and breakdown strength drop ($\Delta\tau_b$), which together define the fracture energy. During the dynamic rupture process, the fracture energy is essentially consumed by balancing the strain energy release supplied near the rupture front [*Madariaga and Olsen*, 2000]. $\Delta\tau_b$ is the difference between the static shear strength before the rupture ($\tau_s$) and the residual dynamic strength ($\tau_d$). $D_c$ is the amount of slip required for the stress to reach the dynamic stress level, after dropping from the static strength.

[52] It is difficult to constrain $\Delta\tau_b$ and $D_c$ from the field observations. The strength depends directly on the effective normal stress, but effective normal stress on the fault are unknown because we do not know the fluid pore pressure on the fault. It can be measured by in-situ experiments at shallow depth, but it is hard to measure it at seismogenic depth on the plate interface. Slip-weakening distance is a more complex parameter. It might not be a local material-dependent parameter, but a dynamic one that depends on the ongoing rupture process. Therefore, we can only measure this parameter during the slipping. The fracture energy, which can be defined by $\Delta\tau_b$ and $D_c$, is mostly a physical and numerical concept, and we cannot directly measure its value in the nature. Therefore, we need to assume these parameters by referring to available observations.

#### 3.3.1. Shear Strength Setting

[53] Since we set $\tau_d$ by equation (1), we need the shear strength $\tau_s$ to get the distribution of $\Delta\tau_b$. $\tau_s$ controls the onset of the slip. In the Coulomb friction framework, it depends on the normal stress that clamps the fault. The normal stress depends on the local stress field, and can be strongly modified by pore pressure, both statically and dynamically. These physical quantities are likely to vary greatly over the subduction interface.

[54] In addition, in the process zone at crack tip, cohesive forces are commonly introduced to prevent strong and unphysical stress singularities ahead of the crack. In discrete modeling, the distance between broken and unbroken nodes of the fault cannot be smaller than the grid spacing. Therefore, the strength, actually referring to a failure criterion, should be set in regard to the spatial discretization. When the spatial resolution is larger, the failure criterion should be smaller. Depending on the numerical method, the crack tip discretization has different implications. For instance, in finite difference method (FDM), a spatial resolution much smaller than the cohesive zone size is required in order to solve the failure propagation problem properly [e.g., *Day et al.*, 2005]. In the BIEM, this requirement is substantially different, as the method is not based on spatial derivative estimations. Our main requirement is that the time step is sufficiently small so that the weakening curve is properly followed on each single fault element. The stress concentration at the edge of the crack is accurately described in the BIEM, but a spatial resolution issue is actually rising from the fact that the stress intensity decreases away from the edge, and that the size of the elements determines the distance at which the stress concentration is sampled.

[55] For simplicity, because of these numerous uncertainties and lack of physical constrains on the strength distribution, we assume that $\tau_s$ is uniform over the plate interface. Since the fault element breaks when the stress overcomes the strength, the only requirement is to set the strength larger than the initial stress. The fact that we consider a heterogeneous initial stress $\tau_0$ and stress drop $\tau_0 - \tau_d$ produces a heterogeneous distribution of $S$ defined as

$$S = \frac{\tau_s - \tau_0}{\tau_0 - \tau_d} \tag{3}$$

[*Andrews*, 1976]. In the case of uniform strength, $S$-value becomes higher where the initial stress is lower. Thus, the rupture cannot easily propagate away from the loaded area. This is a crude approximation regarding the expected depth-dependency of the friction properties, since the edges of the seismogenic zone will be very difficult to break. However, it is still a reasonable proxy for the computation of the rupture phenomenon, because very little strain energy is released coseismically in these areas. It should be noted that no slip-hardening is considered at the edges of seismogenic zone. A merit of uniform strength assumption is that the rupture can propagate spontaneously inside the loaded area once it started, since $S$ is the smallest there.

[56] An alternative assumption would be a uniform $S$ distribution, provoking a lower strength at shallow and deep depths where the stress drop is low. This might be more realistic at those depths, but it becomes almost impossible to propagate the rupture spontaneously in the seismogenic zone without a strong artificial overshoot, since asperities become very resistant. We computed several models for such homogeneous $S$ for a single Nankai asperity case whose results are shown in Appendix A to discuss the effect of different strength assumptions. Because we are studying the coseismic rupture process, not the loading process (which involves some slip at depth) [see *Hori et al.*, 2004], a uniform strength over a non-uniform initial stress is suitable here.

[57] In this study, we set $\tau_s$ = 8.6 MPa, which is 0.1 MPa larger than the maximum initial stress value. This makes $S$ values ranging from close to 0 in the asperities to more than 5 out of the seimogenic zone.

[58] To avoid unphysical interaction with the free surface, the elements on the plate interface whose depth is shallower than or equal to 3 km, have their strength arbitrary multiplied by a factor of 10. This is to achieve the CFL condition between slab interface elements and the free surface lying above.

#### 3.3.2. $D_c$ Setting

[59] The distribution of $D_c$ is another constitutive parameter. Some debates exist about the physical meaning of $D_c$ [*Marone et al.*, 2009, and references therein]. It is an essential parameter describing the strength breakdown of the fault, depending for instance on fault thickness, gouge structure, and interface rugosity. The main problems regarding $D_c$ estimation is that (1) it depends on many physical parameters, including dynamically varying ones (such as temperature), and (2) it is likely to be scale dependent, therefore it is not easy to extrapolate laboratory measurements to earthquakes.

[60] The scaling of $D_c$ with slip is a very common result of the seismologic source observations [*Mikumo et al.*, 2003; *Tinti et al.*, 2005]. It ranges typically between 20 to 100% of the final slip. It has been demonstrated that this result could be a pure methodological bias [*Guatteri and Spudich*, 2000; *Cocco et al.*, 2009], but such a scaling could exist physically, due to the scale dependence of the fault breakdown process.

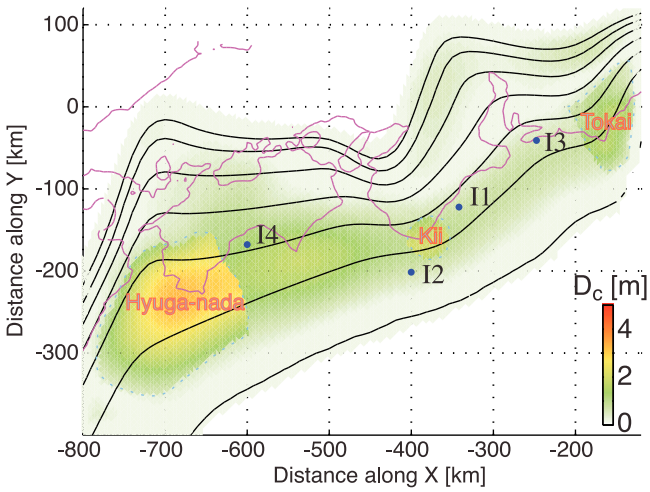


**Figure 7.** Critical slip distance distribution. $D_c$ is assumed to be 20% of slip-deficit for 100 years (Figure 4a). Inside three zones (Hyuga-nada, Kii peninsula, and Tokai) $D_c$ is assumed to be 40% of the slip-deficit. These zones are located inside the positive stress drop area. The locations of the initiation points (I1-I4) are also indicated.

[61] In absence of very strong constraints on $D_c$ value, we consider a reasonable assumption that the scaling exists. Admitting that a strong correlation is likely to be an artefact, we chose a low scaling factor of 20% of the final slip. The order of magnitude of $D_c$ must be adapted to the spatiotemporal resolution of the numerical model. Short length-scale friction breakdown (small $D_c$) cannot be achieved with large time step. In that case, the slip-stress history might undersample the prescribed constitutive behavior, resulting in a different fracture energy. For that reason, we introduced a minimum threshold value for $D_c$ at 0.1 m. Negative slip is considered positive for $D_c$ estimation.

[62] In a spontaneous rupture, the final slip is not imposed. Thus, we assumed

$$D_c(\mathbf{x}) = \max(kB(\mathbf{x}), 0.1) \tag{4}$$

$k$ being a constant equal to 0.20, and $B$ the amount of slip-deficit. This assumption provides a reasonably variable $D_c$ distribution, whose maximum value reaches about 2 m where the stress drop is large, and having a 1 m average value over the seismogenic zone. This is a typical order of magnitude for earthquakes, based on observational estimates. Assuming a scaling of $D_c$ with the slip has the advantage of producing the fracture energy to vary together with stress drop. Other spatial distributions, such as uniform $D_c$, different scaling factor of $D_c$ with slip, and scaling with distance, were tested and their results are shown briefly in Appendix A. These tests suggested that the rupture segmentation could not be achieved using these parametrizations. While the stress drop distribution presents clear asperities, the rupture could easily propagate from one to another, without stopping. The only way to arrest the rupture between asperities was to introduce spatial heterogeneity.

#### 3.3.3. Introduction of $D_c$ Heterogeneity

[63] Since our main interest is to observe the rupture propagation along the Nankai and Tonankai asperities, taking into account the spatial correlations we discussed, we divided the whole Nankai seismogenic zone where the expected stress drop is positive into five regions (Figure 3g). From West to East, these are Hyuga-nada, Nankai, Kii, Tonankai, and Tokai areas. Three of these regions are possible barriers relative to the Nankai and Tonankai asperities. Separating the two asperities, the Kii intersegment is a patch located between the hypocenters of 1944–46 earthquakes, under uplifted area and high Bouguer anomaly. At the western edge, the uplifted cape Ashizuri region with the high Bouguer anomaly is considered as a barrier similar to that in the Kii peninsula. In this study, the Hyuga-nada asperity and the Ashizuri barrier were combined, for simplicity and focusing on the Nankai-Tonankai segments. At the eastern edge, the Tokai region is defined by the area below cape Omae-zaki. Because slip-deficit model is not accurate there, we consider the Tokai region as a barrier. These three regions will be assigned larger fracture energy than the remaining Nankai and Tonankai asperities, through an increase in $D_c$ scaling factor.

$$D_c(\mathbf{x}) = \begin{cases} kB(\mathbf{x}) & (\mathbf{x} \notin \text{barriers}) \\ 2kB(\mathbf{x}) & (\mathbf{x} \in \text{barriers}) \end{cases} \tag{5}$$

The factor of 2 between asperities and barriers is arbitrary, but we set this value after several trials. Figure 7 shows the resulting $D_c$ distribution considered in the following of this paper. The barrier areas, with higher $D_c$, are highlighted and labeled. Such an increase of fracture energy is consistent with the presence of structural complexity below uplifted areas.

### 3.4. Initiation of the Rupture in the Scenarios

[64] We considered 4 different positions for the rupture hypocenter. These points are shown in Figure 7 and listed in Table 1. Points I1 and I2 correspond to the area where the 1944 and the 1946 earthquakes initiated, respectively. Other places have also been identified as possible initiation region for large earthquakes in the past. For instance, the 1707 and 1854 ruptures may have started from the Tokai area. Since we do not consider Tokai area in the present study, we instead considered that the rupture could initiate from the eastern edge of the Tonankai region, as marked by point I3

**Table 1.** Initiation Positions for the Rupture Scenarios

| Point Name | Position | Distance Along $X$[a] (km) | Distance Along $Y$[a] (km) | Depth (km) |
|---|---|---|---|---|
| I1 | 1944 Tonankai hypocenter | −340 | −120 | 15.6 |
| I2 | 1946 Nankai hypocenter | −400 | −200 | 5.5 |
| I3 | eastern edge of Tonankai | −250 | −40 | 14.9 |
| I4 | western edge of Nankai | −600 | −170 | 21.1 |

[a] $X$- and $Y$- coordinates are shown in Figure 2.

(under Ise bay). In addition, we also tested a scenario where rupture starts from the western edge of the Nankai segment (point I4, under Tosa bay), for completeness. For each scenario, one unique initiation place between those four is assumed.

[65] To achieve rupture initiation, the initial stress must be larger than the strength. During the dynamic rupture computation, this excess over the strength leads to the release of the stress following the constitutive relation. In a circular zone with a radius of 25 km around the initiation point, the initial stress is raised up to 0.01 MPa over the local strength. In practice, the distance is measured between the horizontal coordinates of the barycenter of the elements. The radius has been tuned so that the rupture propagates outside of the initiation zone. It was kept at 25 km for all the initiation points for simplicity and homogeneity of the models. However, it means that the overshoot has not been minimized. The initial stress overshoot perturbates the final slip distribution accordingly. A proper way to initiate the rupture would have been to consider a critical state of strength with respect to the initial stress distribution, so that the rupture initiates spontaneously at small scale, and then propagates to the bigger scale we are computing [*Ide and Aochi*, 2005]. This requires an inversion of much finer scale strength distribution, that we did not perform in this study.

## 4. Computation Results

### 4.1. Reproducing the 1944 Tonankai–1946 Nankai Earthquake Sequence

[66] In the first scenario we tested, the rupture was initiated at the hypocenter zone of the 1944 earthquake (I1 in Figure 7), east of Kii peninsula. As shown in Figure 8, the rupture first developed inside the initiation zone, then it propagated bilaterally in the Tonankai asperity. As the rupture initiated at the deeper part of the seismogenic zone, the rupture also propagated upward, while downward propagation was very slow. Because of uniform strength assumption, *S*-value becomes very large (larger than 5) where initial stress is low at the down- and updip edges of the seismogenic zone, while it is typically around 1 at the center of the seismogenic zone where initial stress is the highest. The ruptured area is basically surrounded by strong barriers. But the rupture did propagate a few kilometers inside the negative stress drop area, and its width is wider than the positive stress drop region (so-called seismogenic zone). The rupture propagated easily to the east and finally stopped at the Tokai area where the $D_c$ was increased. Toward the west, the rupture propagated similarly until 20 s when the rupture died below the cape Shiono, in the middle of the segment boundary area. While the rupture could not propagate inside the eastern barrier, half of the segment boundary patch was broken. This is because the initial stress was large enough in the barrier to balance the fracture energy there.

[67] The rupture velocity was measured from the rupture times along the isodepth contour of 12 km. This is a good approximation because the Tonankai asperity is centered around 10 km in depth and the Nankai asperity around 15 km. It took about 60 s for the rupture to reach the eastern edge and the average rupture velocity was 2.3 km/s.

[68] The moment magnitude obtained was 8.3, which is rather large compared to that of the 1944 earthquake (estimated between 7.9 and 8.0). This difference can be explained by two reasons. The maximum slip in the waveform inversions is around 3 m, while the present model reaches 6.5 m due to initial stress overshoot (2.7 m in average). The maximum slip outside the initiation zone is about 3 m. Also, the ruptured area was about twice larger in this model than that derived from the strong motion inversion [*Kikuchi et al.*, 2003]. During the 1944 earthquake, the eastern part of the Tonankai segment was apparently broken slowly [*Tanioka and Satake*, 2001b] without generating strong ground motions, since only geodetic and tsunami waveform inversions required significant slips there, at least in the deeper part [*Sagiya and Thatcher*, 1999; *Tanioka and Satake*, 2001b; *Baba and Cummins*, 2005; *Baba et al.*, 2006]. *Kodaira et al.* [2003] suggested that the subduction of old ridges there could cause the absence of slip in the shallowest part. In our model, no special mechanisms was introduced to produce slow rupture propagation or to represent the ridge subduction, so the rupture simply propagated farther. Together with the slip overshoot at the initiation, this explains the differences in moment magnitude between our model and the observation of the 1944 earthquake.

[69] After the Tonankai rupture scenario, the stress concentrated around the ruptured area. At the western side of Kii peninsula area, where the 1946 Nankai earthquake had initiated, the stress actually increased after this Tonankai rupture scenario. Therefore, we used the final stress distribution of the Tonankai scenario as the initial stress distribution for the Nankai scenario (see Figure 9). We assumed the same constitutive parameters as the Tonankai case. It implicitly assumes that the frictional strength healed inside the previously ruptured area. To start the rupture, we again overshooted the stress up to the static yield stress inside the initiation area (I2 in Figure 7).

[70] The second earthquake rupture initiated at the shallow part of the plate interface and propagated downward during the first 40 s (Figure 9). This propagation was in the in-plane mode. The rupture did not propagate far in the Tonankai area because the stress had already been released by the previous earthquake, while the static strength had recovered. Therefore, after 40 s, the rupture propagated unilaterally to the west, and it reached the large stress asperity located below the cape Muroto. The rupture broke the whole asperity and died when penetrating into the large $D_c$ barrier below the western Shikoku island. The average rupture velocity inside cape Muroto asperity was also very slow, around 2.3 km/s. As in the Tonankai scenario, the rupture widely penetrated above and below the seismogenic zone, whose limit was close to 4.5 MPa initial stress. The slip distribution below the Shikoku is consistent with those of the inversion models [e.g., *Sagiya and Thatcher*, 1999; *Tanioka and Satake*, 2001a]. The magnitude is again overestimated, for the same reasons as for the Tonankai scenario. This time our model was $M_w$ 8.4, while the observation was 8.0.

### 4.2. Predicted Ground Motions: Comparison With Observations

[71] After the 1944–46 earthquakes, coseismic vertical displacements were observed; 0.4-0.6 m uplift at cape Shiono, and about 0.8-1.0 m uplift at cape Muroto [*Thatcher*, 1984; *Ando*, 1975]. We compared these observations with our results, as shown in Figure 10. In cape Shiono region, we

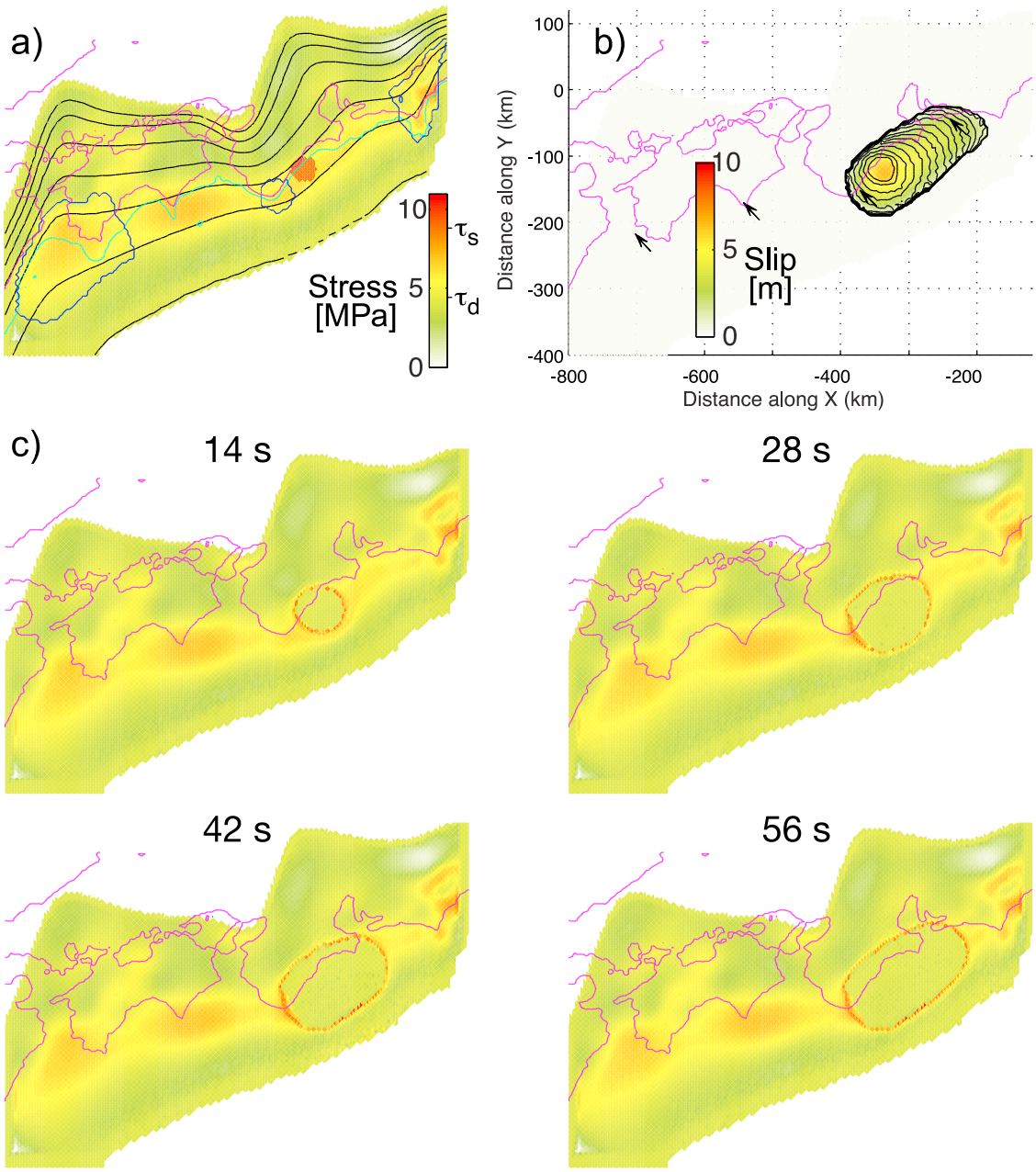


**Figure 8.** Result of the Tonankai-like rupture. (a) Initial shear stress distribution on the fault. Overshooted area for initiation appears in red. Lines indicate: 10 km depth contours of plate boundary (black), coast line (pink), −250 m altitude (light blue), barrier areas where the $D_c$ scaling factor is increased (dark blue). (b) Final slip distribution and rupture time contours every five seconds. Arrows denote the slip direction of the slab. (c) Snapshots of the stress during the rupture propagation.

have 0.16 m subsidence during the Tonankai earthquake and 0.82 m uplift during the Nankai earthquake, resulting in 0.66 m vertical uplift, which is consistent with the observation. The horizontal displacement (not shown here) is in good agreement with *Ando* [1975] in its direction, but our amplitude seems too large, reaching 3 m. For the Nankai scenario, in cape Muroto region, it was 0.45 m uplift in our model, which is lower than the observation. We obtained a 0.35 m horizontal displacement to the east and 0.2 m subsidence at cape Ino, located north of cape Ashizuri, which is consistent with that reported by *Ando* [1975]. It should be pointed out that the location of the hinge line (a boundary between uplift and subsidence regions) is roughly consistent with the observations shown by *Ando* [1975] for the three scenarios (Figure 10).

[72] We could not compare the computed ground motions with those observed (e.g., strong motion waveforms for the Tonankai earthquake [*Kikuchi et al.*, 2003]), because of the significant differences in their frequency range; old seismograms were band-limited and our computation cannot reproduce such high frequency displacements in the present study. To make comparisons, we would need to compute

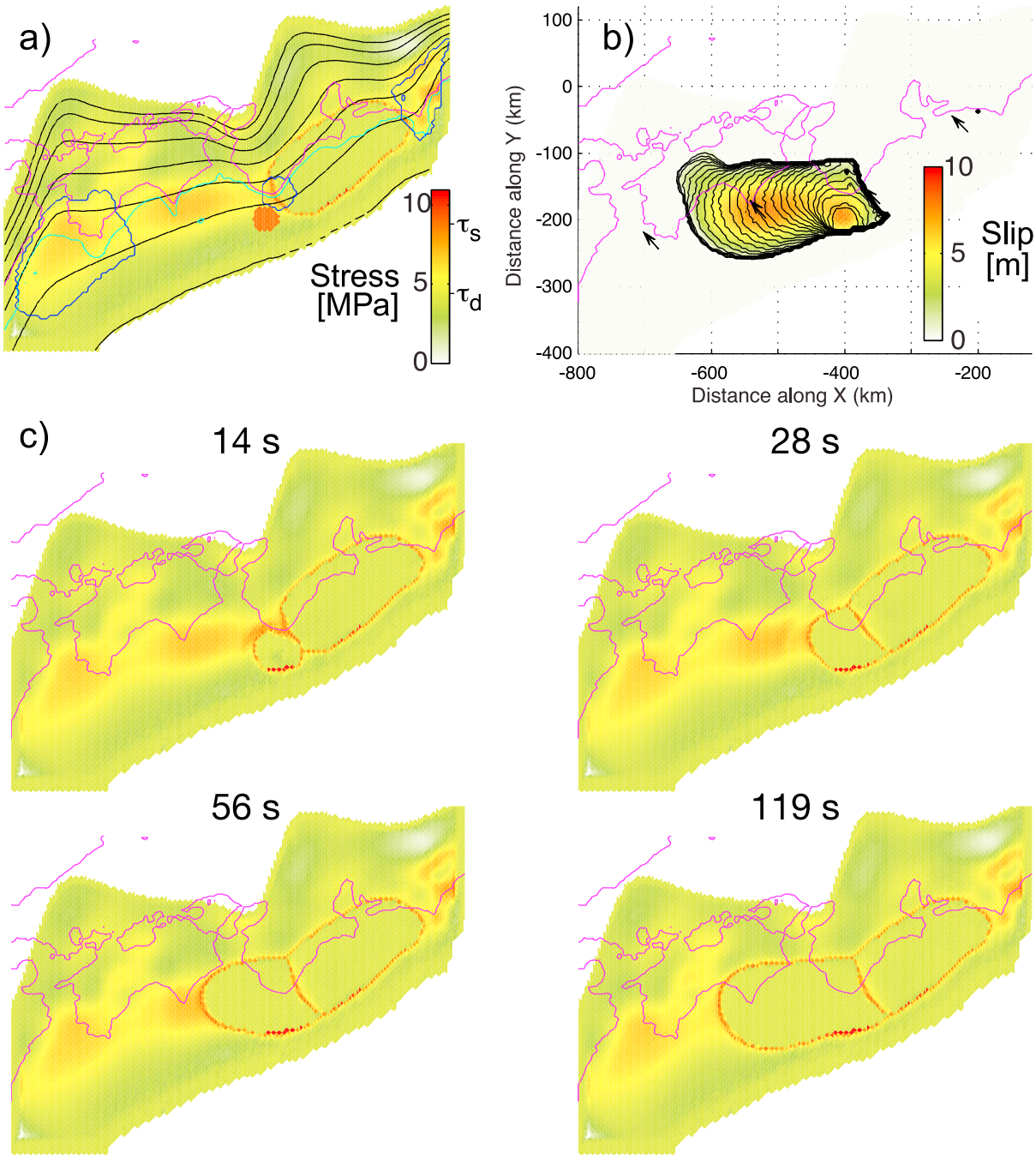


**Figure 9.** Results of the Nankai-like rupture. Legends are the same as Figure 8. Initial stress is the final stress of the Tonankai earthquake shown before.

waveforms with a realistic 3-D velocity structure instead of using halfspace assumption as in the present case.

### 4.3. Other Rupture Scenarios: Giant Earthquakes and Barrier Criticality

[73] Here, we compare the above Tonankai-like scenario to other scenarios using the same initial stress distribution. The difference comes from constitutive parameters that we changed, and initiation location.

[74] First, we investigate the role of the heterogeneity that we introduced at the segment boundary. Now, we assume that $D_c$ scaling is uniform at the segment boundary between the Nankai and Tonankai areas (beneath cape Shiono). The rupture initiates at point I1, the same as in the Tonankai scenario. However, due to the absence of barrier, the whole Nankai-Tonankai region was broken as a single event. This result suggests that the heterogeneity of the constitutive parameters is responsible for the segmentation of the rupture during the earthquakes along the Nankai trough. It also demonstrates that the realistic stress drop distribution we assumed was not sufficient to explain the rupture segmentation, and that we need to validate the constitutive parameters under Kii peninsula.

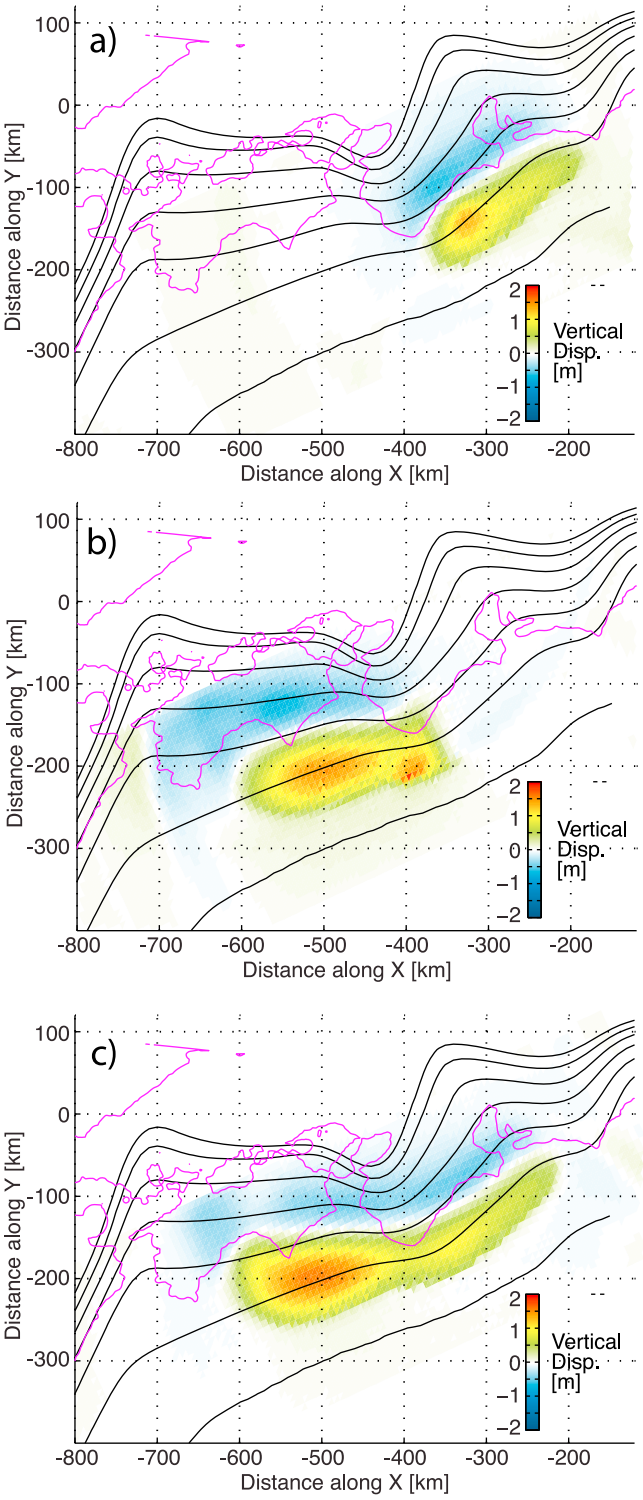


**Figure 10.** Final vertical ground displacements computed at the free surface for (a) Tonankai-like, (b) Nankai-like, and (c) Giant rupture scenarios. These scenarios are shown as h1, h3, and h4 in Table 2, respectively.

[75] We conducted other tests to demonstrate the criticality of the constitutive parameters, by studying the effect of the rupture initiation location. We assumed that the rupture initiates at either I2, I3 or I4 (see Figure 7). No modification was made for the constitutive parameters, so that the Kii peninsula barrier is still set up.

[76] When the rupture initiated at the western edge of the Nankai segment (I4), it broke successively the entire Nankai segment, the segment boundary and the Tonankai segment. It finally produced a giant rupture, as a single $M_w$ 8.6 earthquake. The segment boundary could not stop the rupture coming from the Nankai segment. This giant rupture finally died spontaneously within the Tonankai area, before hitting the Tokai barrier. This scenario (u4 in Table 2) suggests that it is easier for the rupture to break the barrier if the rupture starts far from the segment boundary than close to the boundary. In view of rupture dynamics, this is reasonable because the energy available for the propagation of the rupture depends on the size of the ruptured area [e.g., *Madariaga and Olsen*, 2000].

[77] We then considered that the rupture initiated at I3, the eastern edge of the Tonankai segment (u3 in Table 2). In this case, the rupture could not propagate across the segment boundary. This suggests that it is easier for the rupture to propagate across the barrier starting from the Nankai segment than from the Tonankai segment.

[78] To elucidate factors leading to segmented or single rupture, more detailed parameter space studies were required. Additional scenarios were conducted under a full-space hypothesis to save the computation time, as listed in Table 2. The full-space scenarios reproduced well the results obtained in half-space models for the cases of u1, u3 and u4. In addition to the initiation location, two other parameters were investigated. $k$, the scaling factor of $D_c$, was changed with applying equation (5), as well as the strength level on the Tonankai segment. The results are presented in detail in Appendix B. An interesting result came out when initiating from eastern Tonankai segment (I3): the rupture could jump the Kii peninsula barrier (model b3). This case is shown in Figure 11. These computations show that the behavior of the barrier at segment boundary depends on the distance to initiation.

[79] Investigation of $k$ showed that our assumption of constitutive parameters is a critical case, that may be close to the real conditions, since most of the rupture patterns (1707, 1856, 1944, 1946) observed at Nankai trough were reproduced by the model.

[80] We can summarize our rupture scenarios as the combination of two factors. First, the average fracture energy level with respect to the initial stress distribution determines the capacity of the rupture to stop at the barrier location. This is related to the average energy balance between available strain energy, that depends on the stress drop distribution, and the average fracture energy as specified by the constitutive law. While the stress drop distribution is imposed by slip-deficit rate, the constitutive parameters are not well constrained. We cannot examine all parameter sets, but we can easily identify two end-member cases for rupture propagation: (1) only segmented scenarios are produced when the fracture energy is large, and (2) only giant rupture are produced when fracture energy is small. Between these two cases, there is a critical transition.

[81] Second, for a critical parametrization of the constitutive parameters, the sensitivity of the barrier depends on where the rupture initiates. If the rupture initiates far from the

**Table 2.** Parameters and Final Rupture Extent for Rupture Scenarios[a]

| Name | Medium | $k$ (%) | Initiation | Strength | Final Size |
|---|---|---|---|---|---|
| h1 | half | 20 | I1 | uniform | Tonankai |
| h3 | half | 20 | I3 | uniform | Tonankai |
| h4 | half | 20 | I4 | uniform | Nankai + Tonankai |
| u1 | full | 20 | I1 | uniform | Tonankai |
| u2 | full | 20 | I2 | uniform | Nankai + delayed Tonankai |
| u3 | full | 20 | I3 | uniform | Tonankai |
| u4 | full | 20 | I4 | uniform | Nankai + Tonankai |
| a1 | full | 20 | I1 | step | Tonankai + Nankai |
| a2 | full | 20 | I2 | step | Nankai + Tonankai |
| b1 | full | 25 | I1 | step | Tonankai |
| b2 | full | 25 | I2 | step | Nankai + delayed Tonankai |
| b3 | full | 25 | I3 | step | Tonankai + Nankai |
| b4 | full | 25 | I4 | step | Nankai + Tonankai |
| c1 | full | 30 | I1 | step | Tonankai |
| c2 | full | 30 | I2 | step | (No rupture) |

[a]Here 'half' stands for half-space, and 'full' for full-space. $k$ is the scaling factor of $D_c$ defined in equation (4).

Kii peninsula segment boundary, more energy is available for the rupture to cross the barrier, and it becomes a giant earthquake rupture. The results show that many different dynamic scenarios can be generated using a single set of initial condition, by only changing hypocenter position.

[82] With the most critical settings that we used (series u and b in Table 2), we could obtain a giant rupture scenario such as what could have occurred in 1707 [*Matsu'ura et al.*, 2010]; the whole plate interface was broken, initiating at far east of the Tonankai segment. The scenario obtained with a uniform strength (u3 in Table 2) would be rather like the 1854 Tonankai event. The same parametrization, but initiating closer to the Kii peninsula, produces segmented ruptures such as in 1944 and 1946. It is remarkable that we could reproduce giant ruptures by introducing small changes within initial parameters of the 1944–1946 segmented earthquakes scenarios. The model parameters that produce this result seem critical, and thus might be different from the actual state of the plate interface. However, from the point of view of hazard mitigation, this critical state produces a lot of variability in the final size of the rupture. This is one of the typical worst-case situations that should be taken into account for evaluation of seismic risks. Therefore, in the framework of future earthquake anticipation, we should not restrict our analysis to the reproduction of 1940s sequence, but rather consider various possible scenarios and need to discuss their probability.

## 5. Application to the 2011 Tohoku-Oki Earthquake

[83] On March 11, 2011, a giant subduction earthquake ($M_w$9.0) occurred east off Tohoku, northeast Japan. Since this earthquake occurred in another part of Japan that we are studying here, it is a very good target for the evaluation of the proposed technique. We thus applied the above methodology to estimate a dynamic rupture scenario of the 2011 Tohoku-Oki earthquake. Then we compare it with the source models that many researchers estimated from the observations.

[84] In this computation, we used the plate boundary model for Pacific plate [*Hashimoto et al.*, 2004], while the Philippine Sea plate model was used for the Nankai-Tonankai case. Both plate interface models were constructed under the same assumption [*Hashimoto et al.*, 2004]. We used the slip-deficit rate estimated by *Hashimoto et al.* [2009a]. This slip-deficit rate distribution was estimated using the same method as that for the Nankai-Tonankai case. For the Tohoku earthquake, no information was available on the recurrence interval of this earthquake. Thus we tentatively set the recurrence interval to 100 years south of 38.9°N (Y = 432.3). In the north of 39.1°N (Y = 454.5), we assume that slip deficit is accumulated for 50 years, taking into account the 1968 Tokachi-Oki earthquake ($M_w$8.2) [*Mori and Shimazaki*, 1985]. Between 39.1°N and 38.9°N, the slip deficit time is linearly interpolated which might correspond to the 1994 Sanriku-Haruka-Oki earthquake ($M_w$7.7) [*Nakayama and Takeo*, 1997].

[85] The total amount of slip-deficit is proportional to the amount of stress drop, thus it controls the seismic moment of the earthquake. We will discuss later on the recurrence interval of this earthquake. We set the hypocenter location as estimated by Japan Meteorological Agency (38.103°N, 142.860°E, 24 km) [*Japan Meteorological Agency*, 2011]. The last parameters we have to take into account are the constitutive parameters. We again do not have any information on these parameters. Thus, we assume a uniform static strength distribution over the slipped region. Similarly, we assume that slip weakening distance is set at 20 percents of the slip deficit. These choices are the same as those for the Nankai-Tonankai case. In this simulation, we did not introduce any spatial heterogeneities in the constitutive parameters except for the reduction of slip deficit time in the north. This is because we did not have any direct/indirect information that suggested spatial heterogeneities.

[86] In Figure 12a the initial stress distribution estimated from the slip deficit distribution is shown. From this stress map, we can recognize three asperities. The hypocenter we assumed in this computation is located at the southern end of the northern asperity. At the hypocenter, we initiated the rupture by raising the initial stress to the strength level inside

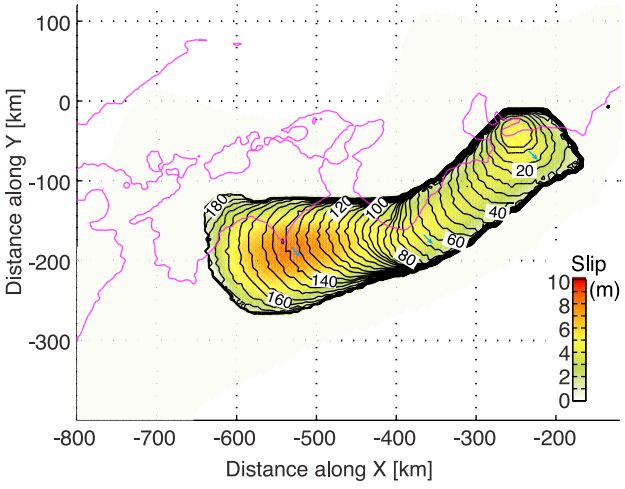


**Figure 11.** Final slip distribution and rupture times of the giant earthquake rupture scenario shown as b3 in Table 2, rupturing from the east. Arrows indicate the direction of slip.

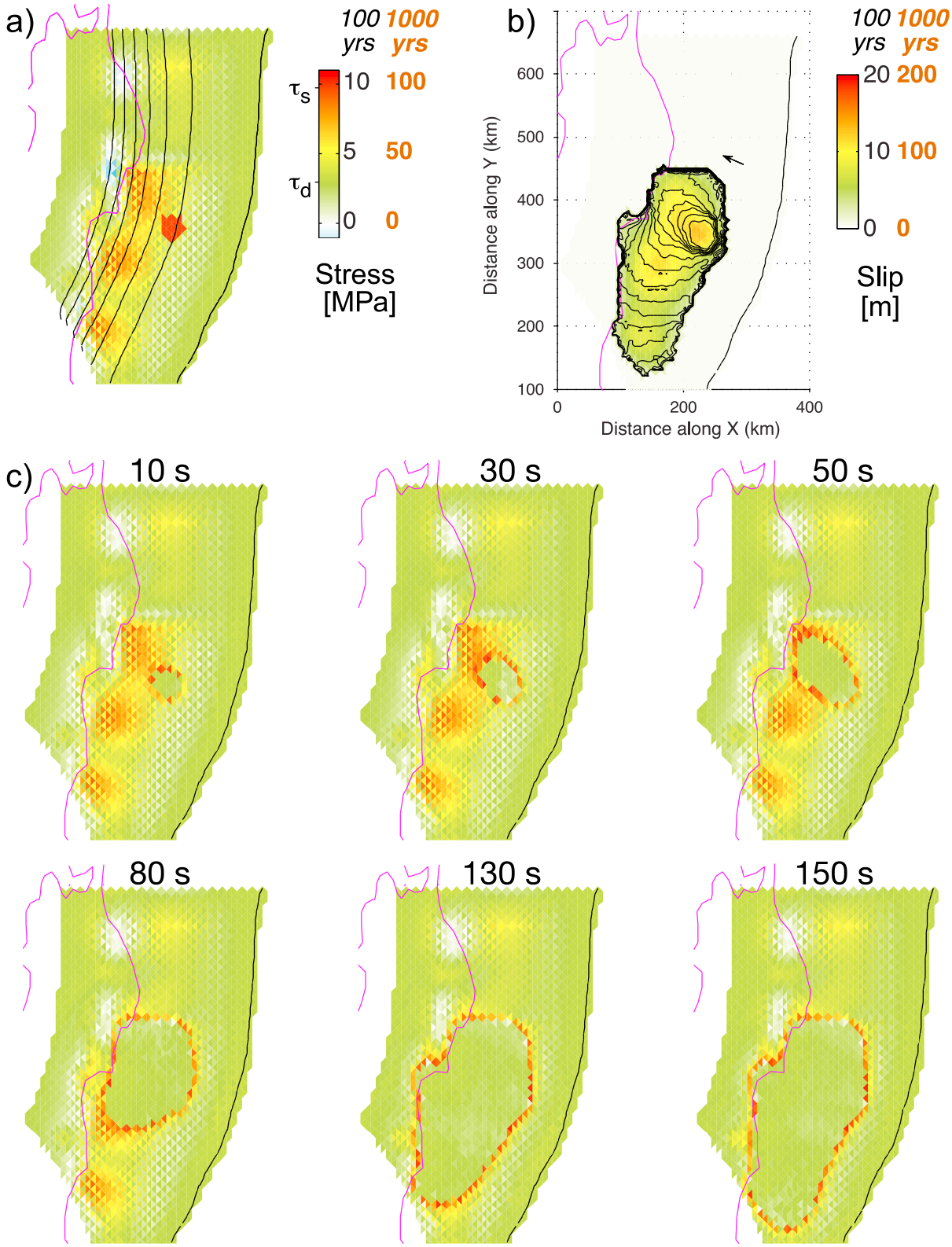


**Figure 12.** Results of the Tohoku rupture scenario. (a) Initial shear stress distribution on the fault. Initiation area is shown in red. Black lines indicate the depth contours of the plate boundary at an interval of 10 km, and pink is the coast line. The black scale in the legend indicates shear stress level for 100 years loading and brown is for 1000 years loading. (b) Final slip distribution. The scales of the legend are again black for 100 years loading and brown for 1000 years loading. The rupture time contours are plotted every 10 s. Arrows denote the slip direction of the slab. (c) Snapshots of the stress during the rupture propagation. Scales are the same as those in Figure 12a.

the initiation zone. Then rupture started to propagate outside the initiation zone.

[87] Rupture front contours and snapshots of the shear stress distribution are shown in Figures 12b and 12c. The rupture first propagated to the north to release the accumulated stress in the northern asperity. Once the rupture propagated in the entire region of the northern asperity, the rupture started to propagate to the south to break the central asperity after about 50 s. Then the rupture continued to propagate to the southern asperity. After the stress in the southern asperity was released completely, the rupture terminated. Total rupture time was about 150 s. These rupture propagation time is more or less similar to the observations [e.g., *Ide et al.*, 2011; *Suzuki et al.*, 2011; *Lee et al.*, 2011]. Therefore, in our modeling, we can say that rupture propagation time can be estimated reasonably as far as we know in advance the rupture initiation point.

[88] Regarding the total seismic moment, it was much smaller than the observation. Apparently, a 100 years recurrence interval was too short to accumulate the stress released during the 2011 Tohoku-Oki earthquake. To fit the observed total seismic moment, we have to assume 10 times more accumulation time for the same slip deficit rate. With 1000 years, we got a total moment of $3.12 \times 10^{22}$ Nm ($M_w$ 9.0). This time period is consistent with that estimated from the Tsunami deposit analysis [*Minoura et al.*, 2001]. It should be noted that since the amount of final slip and thus the stress drop is linearly proportional to the accumuration time of slip deficit, we can interpret the 100 years result as that of 1000 years as shown in Figure 12, as far as we assume that the proportional constant $k$ in equation (4) is the same.

[89] In this case, one may feel that shear strength becomes too high. But it should be noted that if effective normal stress, which is the normal stress value reduced by pore pressure, is high enough and a typical coefficient of friction is assumed, shear strength can be of the same order of the lithostatic stress. *Yoshida and Kato* [2011] proposed a model to achieve such high normal stress condition. In the present case, we believe that a very high stress drop should be required to generate such huge amount of slip reported in several recent articles [e.g., *Sato et al.*, 2011], which automatically requires high shear strength values there.

[90] By the application of the proposed technique to the real data, we recognized that accumulation time of slip deficit and hypocenter location should be important parameters to make the predicted scenarios useful. In other words, as far as we make reasonable assumptions for these parameters, the computed scenarios could be useful for the reduction of future disasters caused by huge subduction earthquakes.

## 6. Discussions

[91] Rupture scenarios will help to mitigate the future disasters. However, the rupture simulation still have limits, due to the lack of knowledge about constitutive parameters.

### 6.1. Seismic Hazard Implications

[92] In our model, the final size of the rupture can change dramatically from one scenario to the other, because the segmentation appeared as a dynamic feature, i.e. the final slip area depends also on the temporal growth of the ruptured area. The conditional segmentation is caused mainly by the particular and critical parameter set we selected. However, we believe that the parameter distributions we used are one of the most realistic ones based on available observations. Our results further suggest that an earthquake initiating inside the Tokai area, which we did not consider here but is expected due to the presence of a seismic gap, can break the entire subduction zone. This scenario requires that the rupture propagates through the Tokai area and complete Tonankai segment, before facing the Kii peninsula barrier. The situation is not unusual. For instance, the 2010 Maule, Chile, earthquake initiated inside an identified gap where no large earthquake occurred since 1835, and continued to propagate where the 1928 earthquake had ruptured, even producing the largest displacements there [*Lorito et al.*, 2011].

### 6.2. Model Limitations

[93] For the purpose of strong ground motions prediction, high frequency ground motions higher than 1 Hz are important. Unfortunately, our rupture models cannot produce high frequency radiation because we used a smooth slip-deficit distribution over a smooth plate interface. To reproduce high frequency radiation, we need to incorporate smaller scale features, such as a more detailed plate interface geometry and a fine description of constitutive parameters. In addition, it would be interesting to take into account a more precise free surface topography, to improve the interaction between the rupture front and the radiated waves.

[94] Another issue is the estimation of the slip-deficit along the seismogenic zone. For instance, in the Hyuga-nada asperity, the 100 years recurrence interval, considered reasonable for the Nankai and Tonankai segments, might be too long for the estimation of the slip-deficit in this area [see *Yoshioka*, 2007]. We also know that there is a 20 years delay between the last Nankai-Tonankai events and the large recent events in Hyuga-nada area (1961 and 1968), so we should examine the spatial variation of the loading time, in addition to the temporal variation of the slip-deficit rate.

[95] At this moment, taking into account the uncertainties and limitations that we have, the above fine-scale modeling was not feasible. This is one of the reasons why we did not include the secondary segments recognized in the traditional segmentation (A-D in Figures 3f and 3g) [*Ando*, 1975; *Sugiyama*, 1994] into the simple segmentation model used here.

### 6.3. Relation Between Uplift and Plate Interface Properties

[96] A correlation between the seismic asperities and the morphology has been proposed [e.g., *Sugiyama*, 1994; *Wells et al.*, 2003]. However, the link between the surface morphology and the slab properties has not been clearly explained yet. We hypothetized that the long-term morphology has been created by deep-under-plating, thus, related to the internal structure of the wedge. Then, the wedge structure could be responsible for the coseismic rupture segmentation at the plate interface. These structural features of the plate interface are not directly supported by observations, since most seismic surveys are done at shallow depth and cannot describe in details the structures at seismogenic depths [e.g., *Nakanishi et al.*, 2002; *Ito et al.*, 2009].

[97] Some relevant information comes from surface or sub-surface observations. *Okamura* [1989, 1990] studied the

coverage of Quaternary sediments on the shelf slope at different locations. He reported that the cape uplifted and that the slope of the shelf at forearc basin subsided. Interestingly, the basement of the shelf slope in the Kii channel exhibits a seaward rotation with time [*Okamura*, 1989, Figure 11], indicating that the bank is formed by upward motion of the inland shelf combined with downward motion of the forearc basin. It suggests that the bank morphology is produced by ongoing tectonic activity, rather than being inherited from an older stage of deformation. It implies the presence of active structures in the deeper wedge that are compatible with the long-term morphology observed, such as shown in our structural interpretation below the peninsulas (Figure 5b).

### 6.4. Barrier Type

[98] One of the characteristic features of the Nankai subduction zone is the conditionality of the Kii peninsula barrier, which was broken coseismically in 1707 or stopped the rupture in 1856 and 1944. The conditionality of the Kii peninsula barrier is associated with large slip-deficits, or large coupling, in agreement with *Konca et al.* [2008] and *Kaneko et al.* [2010] who found that low coupling areas are more likely permanent barriers. We could obtain a similar behavior in the modeling by considering an increase of $D_c$ at the barrier, which preserve the slip-weakening behavior. It ensures large coseismic slip in the barrier (no gap between 1944 and 1946 ruptures). Therefore, this barrier seems essentially different from the rate-strengthening ones found in other subduction zones [*Perfettini et al.*, 2010; *Victor et al.*, 2011], characterized by little coseismic slip inside the barrier. In addition, while velocity-strengthening barriers are usually associated with lower interseismic coupling than the asperities are [*Kaneko et al.*, 2010], the barrier below the Kii peninsula accumulated larger slip-deficits than the neighboring Tonankai asperity in the present case.

[99] There seems to be a significative difference in the barrier type between velocity-strengthening and slip-weakening modeling, especially, in the post seismic deformation and interseismic strain accumulation. However, we cannot rule out any of these hypotheses from available observations because there are no significant differences in the coseismic behavior. But in the postseismic stage after a large earthquake along the Nankai Trough, these two types of heterogeneities might behave differently. Afterslip distribution in the Kii peninsula boundary would favor a velocity-strengthening behavior, while its absence might indicate a slip-weakening barrier type.

[100] It should be noted that the initial state of the barrier is the same for segmented or giant ruptures in our modeling. Whether the rupture overcomes the barrier or not depends only on the slip history of the current rupture. By keeping the initial condition constant, our modeling demonstrated that purely dynamic effects affect the breaking of barriers.

## 7. Conclusions

[101] We proposed several dynamic rupture scenarios for the earthquakes along the Nankai trough using the interseismic slip-deficit rate distribution. The slip-deficit is used for the estimation of the coseismic stress drop distribution, which is crucial in the rupture propagation and the generation of strong ground motions. As a consequence, the dynamic rupture scenarios could capture the essential features of the seismic source, such as the moment release, the rupture propagation, and the seismic wave radiation. Although the predictions are limited to the generation of low frequency waves because of rather smooth parametrization in our modeling scheme, it could be useful for the prediction of tsunami and long period strong ground motions. At least, since the coseismic stress drop distribution is linearly related to the final slip distribution, the worst scenario can be predicted through the dynamic rupture simulation.

[102] Along the Nankai subduction zone, we obtained the segmentation of the rupture by introducing lateral variations in the constitutive parameters. The regional heterogeneity in these parameters was introduced based on the lateral variations of geophysical data and the seismogenic asperities. We modeled regional barriers by increasing $D_c$ while strength is assumed to be uniform on the plate interface. In the present computation, the barrier stops the rupture dynamically when the rupture was initiated close to it, while it breaks when the rupture comes from far away. We obtained both segmented rupture scenarios like the sequence of 1944–1946 events, and a giant earthquake rupture like the 1707 earthquake, with the same constitutive parameter and stress accumulation but changing the initiation location. The present work emphasizes the need for investigations on the quantification of the constitutive parameters in the Nankai subduction zone. For hazard mitigation purposes in southwestern Japan, efforts should be concentrated on Kii peninsula.

## Appendix A: Friction Parameter Tests

[103] To understand the influence of the constitutive parameters on the segmentation of the rupture such as spontaneous arrest at the edge of the asperity, we tested two series of settings: constant $S$ (see equation (3)) and constant $\tau_S$ (shear strength) along the plate interface. For efficient computations, those tests were conducted under full-space condition and on the western part of the plate interface (the Hyuga-nada and the Nankai asperities). We estimated the stress drop distribution for the full-space condition from slip-deficit rate in the same way that for the half-space case. The amount of stress drop for full-space was larger than that for the half-space.

[104] When $S$ is constant over the plate interface, $\tau_S$ is proportional to the stress drop. $\tau_S$ becomes small at the edge of asperities, and slip-strengthening behavior occurs where stress drop is negative. The rupture is initiated by decreasing the strength down to the initial stress on an area with a radius of 25 km, followed by an initial stress overshoot of 0.01 MPa over an area with radius 10 km. The epicenter is located in the Nankai asperity. We studied different $S$-values, and different $D_c$ scaling, as listed in Table A1. Tested $S$-values are 1.0, 1.5 and 2.0 while $D_c$ values are set to 33%, 17%, and 10% of the slip-deficit. As shown in Figure A1a, the rupture breaks almost entire plate surface in all cases because of the low resistance at the edge of the asperity. It was impossible to stop the rupture between the asperities without introducing additional heterogeneity there. We could stop the rupture by introducing different $D_c$ scaling coefficient or $S$ value between asperities. In that case, the rupture dies gradually in the area where the fracture energy becomes larger.

**Table A1.** Model Configuration Tested in Uniform $S$ Cases Shown in Figure A1[a]

| Name | $k$ (%) | $S$ |
|---|---|---|
| hm1 | 10 | 1.0 |
| hm2 | 10 | 1.5 |
| hm3 | 10 | 2.0 |
| hm4 | 17 | 1.0 |
| hm5 | 17 | 1.5 |
| ht1 | 17 → 33 | 1.5 |
| ht2 | 17 → 33 | 1.5 → 2.0 |

[a]The parameters $k$ and $S$ are defined in equations (3) and (4), respectively. The arrow indicates a change from the first asperity to the second one.

[105] In the second series of the tests, $\tau_S$ is assumed to be constant over the fault plane. This is the situation we used for the Nankai-Tonankai rupture scenarios. Here, the initiation is acchieved by lowering the strength level to 0.1 MPa below the initial shear stress in the initiation zone. In this series, we tested several $D_c$ distributions. We used a constant $D_c$ ($D_c$ = 1 m), a scaling with slip-deficit ($D_c = 0.17B(\mathbf{x})$), and a scaling with the distance $L(\mathbf{x})$ from the hypocenter ($D_c = 4 \times 10^{-5} L(\mathbf{x})/(S+1)$). Again, the rupture breaks all the asperities, except in the case of $D_c$ scaling with rupture propagation distance. Figure A1b shows a comparison of rupture propagation time between these different $D_c$ setting models.

[106] From the above two series of computations, we could not get a segmented rupture model such as the Nankai-Tonankai earthquakes sequence. To achieve a segmented rupture, we need to introduce some sort of heterogeneity in the constitutive parameters. For instance, with the introduction of an abrupt increase in $D_c$, we obtained a smooth arrest of the rupture inside the higher fracture energy area (models ht1 and ht2 in Table A1).

[107] These models brought about some interesting insights for the study of the Nankai-Tonankai rupture segmentation. The lateral segmentation of the rupture is difficult to obtain using only the heterogeneous stress drop distribution.

## Appendix B: Nankai-Tonankai Scenarios Using Full-Space Modeling

[108] We conducted additional rupture scenarios under a full-space boundary condition, by neglecting the contribution from the free surface (i.e. by removing the free surface

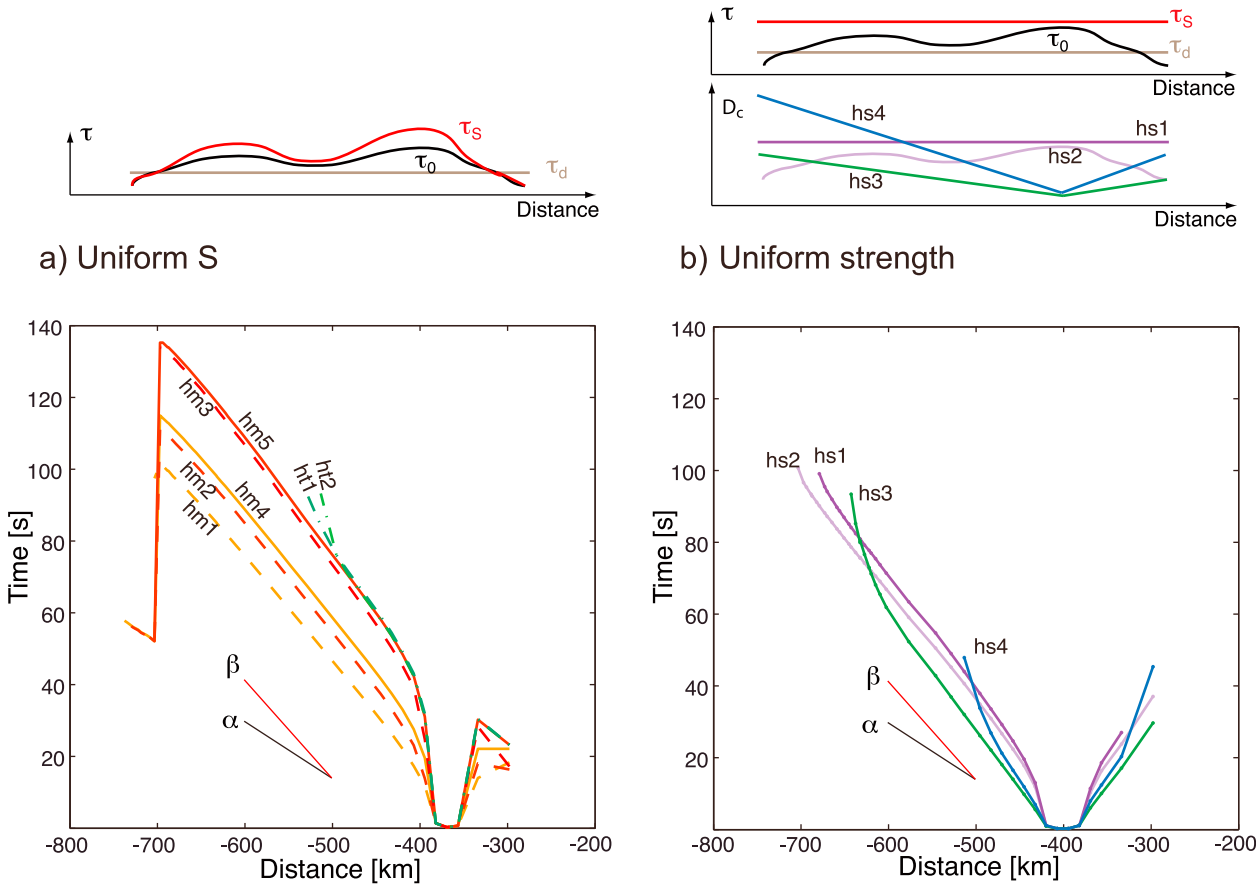


**Figure A1.** Rupture front propagation over the western asperities. $\alpha$ and $\beta$ refer to P and S wave velocity, respectively. The front position is monitored along east–west axis at points lying between 14.5 and 15.5 km depth. Top pictures schematize the lateral variations of the parameters. (a) Uniform $S$ assumed. Tested $S$ and $D_c$ scaling values are shown in Table A1. Only sudden change between the two asperities manages to stop the rupture. (b) Uniform strength is assumed. $D_c$ setting is changing. An increase of $D_c$ makes the rupture die.

elements). This accelerated the computation time, allowing to investigate initial parameter variations. We reestimated the stress drop distribution for full-space rupture cases. As pointed out by *Hok and Fukuyama* [2011], for a given final slip distribution, the stress change is larger in full-space than in half-space. This effect is significant at shallow depth. However, the relative lateral variations which control the segmentation are very similar. In these full-space scenarios, since the strength level is ajusted, the resulting $S$ distribution is similar between full- and half-space cases. The uniform $\tau_s$ becomes 10.5 MPa. Due to variations of plate convergence rate along the trench, the stress is lower on the Tonankai asperity than on the Nankai asperity. Using uniform strength results in a different $S$ level between the segments. To reduce this effect, we also considered a step-like strength distribution, in which $\tau_s$ decreases from 10.5 MPa on the western Nankai segment down to 9 MPa on the eastern part. The reduction was applied only in the positive stress drop area. The transition is linear, and occurs between $y = -480$ km and $y = -450$ km. This step-like $\tau_s$ model produces more similar $S$ distributions on each segment. Other settings such as initiation procedure and $D_c$ settings are the same as described in section 3. We tested three values for the scaling factor $k$ (20%, 25%, and 30%) defined in equations (4) and (5).

[109] The final extent of the rupture obtained for those various parameter sets are shown in Table 2. Similar results were obtained between the full-space and half-space cases (models u1, u3, u4 and h1, h3, h4 in Table 2), showing that the criticality of the Kii peninsula intersegment area is qualitatively the same. One difference is the average rupture velocity, which is larger in the u4 (3.1 km/s), than in the h4 (2.6 km/s). It shows that we cannot quantitatively convert half-space models into full-space ones. However, no difference was observed for Tonankai cases (between u1 and h1, or u3 and h3): maximum sliding velocity and rupture times were almost the same.

[110] From the comparison between u1-4 and b1-4 in Table 2, similar ruptured areas are obtained depending on the initiation position and critical behavior of the barrier beneath Kii peninsula has been observed in both cases. It should be noted that in models b1-4, we raised $k$ to 25% to set appropriate fracture energy comparing to models u1-4. If we decrease (a1, a2) or increase (c1, c2) the fracture energy, the final rupture area changes. When $k$ is decreased (a1, a2), the intersegment barrier is not slowing or arresting the rupture. On the contrary, increasing $k$ (c1, c2) yields to failing initiating the rupture. From the models b1-4 we can see that the dynamic segmentation depends on the distance between the initiation location and the Kii peninsula barrier.

[111] **Acknowledgments.** Valuable comments and suggestions by two anonymous reviewers were quite helpful. This work was supported by the CREST project promoted by Japan Science and Technology Agency, entitled "Integrated Predictive Simulation System for Earthquake and Tsunami Disaster" and the NIED project entitled "Development on Crustal Activity Prediction Technique."

## References

Ando, M. (1975), Source mechanisms and tectonic significance of historical earthquakes along the Nankai Trough Japan, *Tectonophysics*, *27*, 119–140.

Ando, R., R. Nakata, and T. Hori (2010), A slip pulse model with fault heterogeneity for low?frequency earthquakes and tremor along plate interfaces, *Geophys. Res. Lett.*, *37*, L10310, doi:10.1029/2010GL043056.

Andrews, D. J. (1976), Rupture velocity of plain strain shear crack, *J. Geophys. Res.*, *81*(32), 5679–5687.

Ariyoshi, K., T. Hori, J.-P. Ampuero, Y. Kaneda, T. Matsuzawa, R. Hino, and A. Hasegawa (2009), Influence of interaction between small asperities on various types of slow earthquakes in a 3-D simulation for a subduction plate boundary, *Gondwana Res.*, *16*(3–4), 534–544, doi:10.1016/j.gr.2009.03.006.

Baba, T., and P. R. Cummins (2005), Contiguous rupture areas of two Nankai Trough earthquakes revealed by high-resolution tsunami waveform inversion, *Geophys. Res. Lett.*, *32*, L08305, doi:10.1029/2004GL022320.

Baba, T., P. R. Cummins, T. Hori, and Y. Kaneda (2006), High precision slip distribution of the 1944 Tonankai earthquake inferred from tsunami waveforms: Possible slip on a splay fault, *Tectonophysics*, *426*, 119–134.

Brown, K. M., A. Kopf, M. B. Underwood, and J. L. Weinberger (2003), Compositional and fluid pressure controls on the state of stress on the Nankai subduction thrust: A weak plate boundary, *Earth Planet. Sci. Lett.*, *214*, 589–603, doi:10.1016/S0012-821X(03)00388-1.

Cocco, M., E. Tinti, C. Marone, and A. Piatanesi (2009), Scaling of slip weakening distance with final slip during dynamic earthquake rupture, in *Fault-Zone Properties and Earthquake Rupture Dynamics*, edited by E. Fukuyama, chap. 7, pp. 163–186, Elsevier, Burlington, Mass.

Day, S. M., L. A. Dalguer, N. Lapusta, and Y. Liu (2005), Comparison of finite difference and boundary integral solutions to three-dimensional spontaneous rupture, *J. Geophys. Res.*, *110*, B12307, doi:10.1029/2005JB003813.

Dominguez, S., J. Malavieille, and S. E. Lallemand (2000), Deformation of accretionary wedges in response to seamount subduction- Insights from sandbox experiments, *Tectonics*, *19*, 182–196.

El-Fiky, G., and T. Kato (2006), Secular crustal deformation and interplate coupling of the Japanese Islands as deduced from continuous GPS array, 1996–2001, *Tectonophysics*, *422*, 1–22.

Fukuyama, E., and R. Madariaga (1998), Rupture dynamics of a planar fault in a 3D elastic medium: Rate- and slip-weakening friction, *Bull. Seismol. Soc. Am.*, *88*, 1–17.

Fukuyama, E., and T. Mikumo (2006), Dynamic rupture propagation during the 1891 Nobi, central Japan, earthquake: A possible extension to the branched faults, *Bull. Seismol. Soc. Am.*, *96*, 1257–1266.

Furumura, T., K. Imai, and T. Maeda (2011), A revised tsunami source model for the 1707 Hoei earthquake and simulation of tsunami inundation of Ryujin Lake, Kyushu, Japan, *J. Geophys. Res.*, *116*, B02308, doi:10.1029/2010JB007918.

Geological Survey of Japan (1992a), Geological map of Japan, in *Geological Atlas of Japan*, 2nd ed., Asakura Shoten, Tokyo.

Geological Survey of Japan (1992b), Gravity anomaly map of Japan and adjoining areas, in *Geological Atlas of Japan*, 2nd ed., Asakura Shoten, Tokyo.

Guatteri, M., and P. Spudich (2000), What can strong-motion data tell us about slip-weakening fault-friction laws?, *Bull. Seismol. Soc. Am.*, *90*(1), 98–116.

Hasegawa, A., J. Nakajima, N. Uchida, T. Okada, D. P. Zhao, T. Matsuzawa, and N. Umino (2009), Plate subduction, and generation of earthquakes and magmas in Japan as inferred from seismic observations: an overview, *Gondwana Res.*, *16*, 370–400, doi:10.1016/j.gr.2009.03.007.

Hashimoto, C., K. Fukui, and M. Matsu'ura (2004), 3-D modelling of plate interfaces and numerical simulation of long-term crustal deformation in and around Japan, *Pure Appl. Geophys.*, *161*, 2053–2068.

Hashimoto, C., A. Noda, T. Sagiya, and M. Matsu'ura (2009a), Interplate seismogenic zones along the Kuril-Japan trench inferred from GPS data inversion, *Nature Geosci.*, *2*, 141–144, doi:10.1038/ngeo421.

Hashimoto, C., T. Sagiya, and M. Matsuura (2009b), Interplate coupling in southwest Japan inferred from GPS data inversion, paper presented at Fall Meeting, Seismol. Soc. of Jpn., Kyoto, Japan.

Heki, K., and S. Miyazaki (2001), Plate convergence and long-term crustal deformation in central Japan, *Geophys. Res. Lett.*, *28*(12), 2313–2316, doi:10.1029/2000GL012537.

Hirose, F., J. Nakajima, and A. Hasegawa (2008), Three-dimensional seismic velocity structure and configuration of the Philippine Sea slab in southwestern Japan estimated by double-difference tomography, *J. Geophys. Res.*, *113*, B09315, doi:10.1029/2007JB005274.

Hirose, H., and K. Obara (2005), Repeating short- and long-term slow slip events with deep tremor activity around Bungo channel region, southwest Japan, *Earth Planets Space*, *57*, 961–972.

Hirose, H., K. Hirahara, F. Kimata, N. Fujii, and S. Miyazaki (1999), A slow thrust slip event following the two 1996 Hyuganada Earthquakes beneath the Bungo Channel, southwest Japan, *Geophys. Res. Lett.*, *26*(21), 3237–3240, doi:10.1029/1999GL010999.

Hok, S., and E. Fukuyama (2011), A new BIEM for rupture dynamics in half-space and its application to the 2008 Iwate-Miyagi Nairiku earthquake, *Geophys. J. Int.*, *184*(1), 301–324, doi:10.1111/j.1365-246X.2010.04835.x.

Honda, R., and Y. Kono (2005), Buried large block revealed by gravity anomalies in the Tonankai and Nankai earthquakes regions, southwestern Japan, *Earth Planets Space*, *57*, e1–e4.

Hori, T., N. Kato, K. Hirahara, T. Baba, and Y. Kaneda (2004), A numerical simulation of earthquake cycles along the Nankai Trough in southwest Japan: Lateral variation in frictional property due to the slab geometry controls the nucleation position, *Earth Planet. Sci. Lett.*, *228*, 215–226.

Hyndman, R. D., K. Wang, and M. Yamano (1995), Thermal constraints on the seismogenic portion of the southwestern Japan subduction thrust, *J. Geophys. Res.*, *100*(B8), 15,373–15,392.

Ida, Y. (1972), Cohesive force across the tip of a longitudinal-shear crack and Griffith's specific surface energy, *J. Geophys. Res.*, *77*, 3796–3805.

Ide, S. (2010), Striations, duration, migration and tidal response in deep tremor, *Nature Geosci.*, *466*, doi:10.1038/nature09251.

Ide, S., and H. Aochi (2005), Earthquakes as multiscale dynamic ruptures with heterogeneous fracture surface energy, *J. Geophys. Res.*, *110*, B11303, doi:10.1029/2004JB003591.

Ide, S., A. Baltay, and G. C. Beroza (2011), Shallow dynamic overshoot and energetic deep rupture in the 2011 Mw 9.0 Tohoku-Oki earthquake, *Science*, *332*(6036), 1426–1429, doi:10.1126/science.1207020.

Ike, T., G. F. Moore, S. Kuramoto, J. Park, Y. Kaneda, and A. Taira (2008), Variations in sediment thickness and type along the northern Philippine Sea plate at the Nankai trough, *Island Arc*, *17*(3), 342–357, doi:10.1111/j.1440-1738.2008.00624.x.

Ishibashi, K. (1981), Specification of a soon-to-occur seismic faulting in the Tokai district, central Japan, based upon seismotectonics, in *Earthquake Prediction*, *Maurice Ewing Ser.*, vol. 4, edited by D. W. Simpson and P. G. Richards, pp. 297–332, AGU, Washington, D. C.

Ishibashi, K. (2004), Status of historical seismology in Japan, *Ann. Geofis.*, *47*(2–3), 339–368.

Isozaki, Y., K. Aoki, T. Nakama, and S. Yanai (2010), New insight into a subduction-related orogen: A reappraisal of the geotectonic framework and evolution of the Japanese Islands, *Gondwana Res.*, *18*(1), 82–105, doi:10.1016/j.gr.2010.02.015.

Ito, T., and M. Hashimoto (2004), Spatiotemporal distribution of interplate coupling in southwest Japan from inversion of geodetic data, *J. Geophys. Res.*, *109*, B02315, doi:10.1029/2002JB002358.

Ito, T., et al. (2009), Crustal structure of southwest Japan, revealed by the integrated seismic experiment Southwest Japan 2002, *Tectonophysics*, *472*, 124–134, doi:10.1016/j.tecto.2008.05.013.

Japan Meteorological Agency (2011), Monthly report on earthquakes and volcanoes in Japan March 2011, p. 60, Tokyo. (Available at http://www.seisvol.kishou.go.jp/eq/gaikyo/monthly201103.pdf, last access on 15 Aug. 2011.)

Kanamori, H. (1972), Tectonic implications of the 1944 Tonankai and the 1946 nankaido earthquakes, *Phys. Earth Planet. Inter.*, *5*, 129–139.

Kaneko, Y., J.-P. Avouac, and N. Lapusta (2010), Towards inferring earthquake patterns from geodetic observations of interseismic coupling, *Nature Geosci.*, *3*, 363–369, doi:10.1038/ngeo843.

Kikuchi, M., M. Nakamura, and K. Yoshikawa (2003), Source rupture processes of the 1944 Tonankai earthquake and the 1945 Mikawa earthquake derived from low-gain seismograms, *Earth Planets Space*, *55*, 159–172.

Kimura, G., Y. Kitamura, Y. Hashimoto, A. Yamaguchi, T. Shibata, K. Ujiie, and S. Okamoto (2007), Transition of accretionary wedge structures around the up-dip limit of the seismogenic subduction zone, *Earth Planet. Sci. Lett.*, *255*, 471–484, doi:10.1016/j.epsl.2007.01.005.

Kimura, J., R. J. Stern, and T. Yoshida (2005), Reinitiation of subduction and magmatic responses in SW Japan during Neogene time, *Geol. Soc. Am. Bull.*, *117*, 969–986, doi:10.1130/B25565.1.

Kodaira, S., N. Takahashi, A. Nakanishi, S. Miura, and Y. Kaneda (2000), Subducted seamount imaged in the rupture zone of the 1946 Nankai Earthquake, *Science*, *289*(5476), 104–106, doi:10.1126/science.289.5476.104.

Kodaira, S., A. Nakanishi, J.-O. Park, A. Ito, T. Tsuru, and Y. Kaneda (2003), Cyclic ridge subduction at an inter-plate locked zone off central Japan, *Geophys. Res. Lett.*, *30*(6), 1339, doi:10.1029/2002GL016595.

Kodaira, S., T. Hori, A. Ito, S. Miura, G. Fujie, J.-O. Park, T. Baba, H. Sakaguchi, and Y. Kaneda (2006), A cause of rupture segmentation and synchronization in the Nankai trough revealed by seismic imaging and numerical simulation, *J. Geophys. Res.*, *111*, B09301, doi:10.1029/2005JB004030.

Komatsubara, J., and O. Fujiwara (2007), Overview of Holocene tsunami deposits along the Nankai, Suruga, and Sagami troughs, southwest Japan, *Pure Appl. Geophys.*, *164*, 493–507, doi:10.1007/s00024-007-0179-y.

Konca, A. O., et al. (2008), Partial rupture of a locked patch of the Sumatra megathrust during the 2007 earthquake sequence, *Nature*,*456*, 631–635, doi:10.1038/nature07572.

Kumagai, H. (1996), Time sequence and the recurrence models for large earthquakes along the Nankai trough revisited, *Geophys. Res. Lett.*, *23*(10), 1139–1142, doi:10.1029/96GL01037.

Lee, S.-J., B.-S. Huang, M. Ando, H.-C. Chiu, and J.-H. Wang (2011), Evidence of large scale repeating slip during the 2011 Tohoku-Oki earthquake, *Geophys. Res. Lett.*, *38*, L19306, doi:10.1029/2011GL049580.

Le Pichon, X., S. Lallemant, H. Tokuyama, E. Thoue, P. Huchon, and P. Henry (1996), Structure and evolution of the backstop in the eastern Nankai trough area (Japan): Implications for the soon-to-come Tokai earthquake, *Island Arc*,*5*(4), 440–454, doi:10.1111/j.1440-1738.1996.tb00164.x.

Le Pichon, X., S. Mazzotti, P. Henry, and M. Hashimoto (1998), Deformation of the Japanese Islands and seismic coupling: An interpretation based on GSI permanent GPS observations, *Geophys. J. Int.*, *134*(2), 501–514, doi:10.1046/j.1365-246x.1998.00595.x.

Liu, Z., S. Owen, D. Dong, P. Lundgren, F. Webb, E. Hetland, and M. Simons (2010), Integration of transient strain events with models of plate coupling and areas of great earthquakes in southwest Japan, *Geophys. J. Int.*, *181*, 1292–1312, doi:10.1111/j.1365-246X.2010.04599.x.

Llenos, A. L., and J. J. McGuire (2007), Influence of fore-arc structure on the extent of great subduction zone earthquakes, *J. Geophys. Res.*, *112*, B09301, doi:10.1029/2007JB004944.

Lorito, S., F. Romano, S. Atzori, X. Tong, A. Avallone, J. McCloskey, M. Cocco, E. Boschi, and A. Piatanesi (2011), Limited overlap between the seismic gap and coseismic slip of the great 2010 Chile earthquake, *Nature Geosci.*, doi:10.1038/ngeo1073.

Loveless, J. P., and B. J. Meade (2010), Geodetic imaging of plate motions, slip rates, and partitioning of deformation in Japan, *J. Geophys. Res.*, *115*, B02410, doi:10.1029/2008JB006248.

Madariaga, R., and K. B. Olsen (2000), Criticality of rupture dynamics in 3-D, *Pure Appl. Geophys.*, *157*(11–12), 1981–2001, doi:10.1007/PL00001071.

Marone, C., M. Cocco, E. Richardson, and E. Tinti (2009), The critical slip distance for seismic and aseismic fault zones of finite width, in *Fault-Zone Properties and Earthquake Rupture Dynamics*, edited E. Fukuyama, chap. 6, pp. 125–162, Elsevier, Burlington, Mass.

Matsu'ura, R. S., M. Nakamura, and I. Karakama (2010), New proposal of the focal area for 1707 Hoei earthquake, paper presented at Fall Meeting, Seismol. Soc. of Jpn., Hiroshima, Japan.

Mazzotti, S., X. Le Pichon, P. Henry, and S. Miyazaki (2000), Full interseismic locking of the Nankai and Japan-west Kurile subduction zones: An analysis of uniform elastic strain accumulation in Japan constrained by permanent GPS, *J. Geophys. Res.*, *105*(B6), 13,159–13,177, doi:10.1029/2000JB900060.

Mikumo, T., K. B. Olsen, E. Fukuyama, and Y. Yagi (2003), Stress-breakdown time and slip-weakening distance inferred from slip-velocity functions on earthquake faults, *Bull. Seismol. Soc. Am.*, *93*(1), 264–282, doi:10.1785/0120020082.

Minoura, K., F. Imamura. D. Sugawara, Y. Kono, and T. Iwashita (2001), The 869 Jogan tsunami deposit and recurrence interval of large-scale tsunami on the Pacific coast of northeast Japan, *J. Nat. Disas. Sci.*, *13*(2), 83–88.

Miyazaki, S., and K. Heki (2001), Crustal velocity field of southwest Japan: Subduction and arc-arc collision, *J. Geophys. Res.*, *106*(B3), 4305–4326, doi:10.1029/2000JB900312.

Mogi, K. (1990), Seismicity before and after large shallow earthquakes around the Japanese island, *Tectonophysics*, *175*, 1–33.

Moreno, M., M. Rosenau, and O. Oncken (2010), Maule earthquake slip correlates with pre-seismic locking of Andean subduction zone, *Nature*, *467*, 198–202, doi:10.1038/nature09349.

Mori, J., and K. Shimazaki (1985) Inversion of intermediate-period Rayleigh waves for source characteristics of the 1968 Tokachi-Oki earthquake, *J. Geophys. Res.*, *90*(B13), 11,374–11,382.

Nakanishi, A., S. Kodaira, J.-O. Park, and Y. Kaneda (2002), Deformable backstop as seaward end of coseismic slip in the Nankai Trough seismogenic zone, *Earth Planet. Sci. Lett.*, *203*(1), 255–263, doi:10.1016/S0012-821X(02)00866-X.

Nakayama, W., and M. Takeo (1997) Slip history of the 1994 Sanriku-Haruka-Oki earthquake deduced from strong-motion data, *Bull. Seismol. Soc. Am.*, *87*(4), 918–931.

Obara, K. (2010), Phenomenology of deep slow earthquake family in southwest Japan: Spatiotemporal characteristics and segmentation, *J. Geophys. Res.*, *115*, B00A25, doi:10.1029/2008JB006048.

Ohta, K., and S. Ide (2011), Precise hypocenter distribution of deep low–frequency earthquakes and its relationship to the local geometry of the subducting plate in the Nankai subduction zone, *J. Geophys. Res.*, *116*, B01308, doi:10.1029/2010JB007857.

Okamura, Y. (1989), Multi-layered progrational sequences in the shelf and shelf slope of the Southwest Japan forearc, in *Sedimentary Facies in the Active Plate Margin*, edited by A. Taira and F. Masuda, pp. 295–317, TERRAPUB, Tokyo.

Okamura, Y. (1990), Geologic structure of the upper continental slope off Shikoku and Quaternary tectonic mvoement of the outer zone of southwset Japan, *J. Geol. Soc. Jpn.*, *96*(3), 223–237.

Ozawa, S., M. Murakami, M. Kaidzu, T. Tada, T. Sagiya, Y. Hatanaka, H. Yarai, and T. Nishimura (2002), Detection and monitoring of ongoing aseismic slip in the Tokai region, central Japan, *Science*, *298*(5595), 1009–1012, doi:10.1126/science.1076780.

Ozawa, S., T. Nishimura, H. Suito, T. Kobayashi, M. Tobita, and T. Imakiire (2011) Coseismic and postseismic slip of the 2011 magnitude-9 Tohoku-Oki earthquake, *Nature*, *475*, 373–376, doi:10.1038/nature10227.

Park, J. O., T. Tsuru, N. Takahashi, T. Hori, S. Kodaira, A. Nakanishi, S. Miura, and Y. Kaneda (2002), A deep strong reflector of the Nankai accretionary wedge from multichannel seismic data: Implications for under-plating and interseismic shear stress release, *J. Geophys. Res.*, *107*(B4), 2061, doi:10.1029/2001JB000262.

Perfettini, H., et al. (2010), Seismic and aseismic slip on the Central Peru megathrust, *Nature*, *465*, 78–81, doi:10.1038/nature09062.

Rice, J. R. (1993), Spatio-temporal complexity of slip on a fault, *J. Geophys. Res.*, *98*, 9885–9907.

Rosenau, M., and O. Oncken (2009), Fore-arc deformation controls frequency-size distribution of megathrust earthquakes in subduction zones, *J. Geophys. Res.*, *114*, B10311, doi:10.1029/2009JB006359.

Rydelek, P. A., and I. S. Sacks (2003), Triggering and inhibition of great Japanese earthquakes: The effect of Nobi 1891 on Tonankai 1944, Nankaido 1946 and Tokai, *Earth Planet. Sci. Lett.*, *206*(3–4), 289–296, doi:10.1016/S0012-821X(02)01095-6.

Sagiya, T., and W. Thatcher (1999), Coseismic slip resolution along a plate boundary megathrust: The Nankai Trough, southwest Japan, *J. Geophys. Res.*, *104*(B1), 1111–1129, doi:10.1029/98JB02644.

Sato, M., T. Ishikawa, N. Ujihara, S. Yoshida, M. Fujita, M. Mochizuki, and A. Asada (2011), Displacement above the hypocenter of the 2011 Tohoku-Oki earthquake, *Science*, *332*, 1395, doi:10.1126/science.1207401.

Savage, J. C. (1995), Interseismic uplift at the Nankai subduction zone, southwest Japan, 1951–1990, *J. Geophys. Res.*, *100*(B4), 6339–6350, doi:10.1029/95JB00242.

Savage, J. C., and W. Thatcher (1992), Interseismic deformation at the Nankai trough, Japan, subduction zone, *J. Geophys. Res.*, *97*(B7), 11,117–11,135, doi:10.1029/92JB00810.

Sekiguchi, H., M. Yoshimi, H. Horikawa, K. Yoshida, S. Kunimatsu, and K. Satake (2008), Prediction of ground motion in the Osaka sedimentary basin associated with the hypothetical Nankai earthquake, *J. Seismol.*, *12*(2), 185–195, doi:10.1007/s10950-007-9077-8.

Seno, T., S. Stein, and A. Gripp (1993), A model for the motion of the Philippine Sea plate consistent with NUVEL-1 and geological data, *J. Geophys. Res.*, *98*(B10), 17,941–17,948, doi:10.1029/93JB00782.

Shiomi, K., M. Matsubara, Y. Ito, and K. Obara (2008), Simple relationship between seismic activity along Philippine Sea slab and geometry of oceanic Moho beneath southwest Japan, *Geophys. J. Int.*, *173*, 1018–1029, doi:10.1111/j.1365-246X.2008.03786.x.

Song, T. A., and M. Simons (2003), Large trench-parallel gravity variations predict seismogenic behavior in subduction zones, *Science*, *301*(5633), 630–633, doi:10.1126/science.1085557.

Sugiyama, Y. (1994), Neotectonics of southwest Japan due to right-oblique subduction of the Philippine Sea plate, *Geofis. Int.*, *33*(1), 53–76.

Suwa, Y., S. Miura, A. Hasegawa, T. Sato, and K. Tachibana (2006), Interplate coupling beneath NE Japan inferred from three-dimensional displacement field, *J. Geophys. Res.*, *111*, B04402, doi:10.1029/2004JB003203.

Suzuki, W., S. Aoi, H. Sekiguchi, and T. Kunugi (2011), Rupture process of the 2011 Tohoku-Oki mega-thrust earthquake (M9.0) inverted from strong-motion data, *Geophys. Res. Lett.*, *38*, L00G16, doi:10.1029/2011GL049136.

Tabei, T., M. Adachi, S. Miyazaki, T. Watanabe, and S. Kato (2007), Interseismic deformation of the Nankai subduction zone, southwest Japan, inferred from three-dimensional crustal velocity fields, *Earth Planets Space*, *59*, 1073–1082.

Tada, T. (2006), Stress Green's functions for a constant slip rate on a triangular fault, *Geophys. J. Int.*, *164*, 653–669, doi:10.1111/j.1365-246X.2006.02868.x.

Tada, T., and R. Madariaga (2001), Dynamic modelling of the flat 2-D crack by a semi-analytic BIEM scheme, *Int. J. Numer. Methods Eng.*, *50*(1), 227–251, doi:10.1002/1097-0207(20010110)50:1<227::AID-NME166>3.0.CO;2-5.

Taira, A. (2001), Tectonic evolution of the japanese island arc system, *Ann. Rev. Earth Planet. Sci.*, *29*, 109–134, doi:10.1146/annurev.earth.29.1.109.

Tanioka, Y., and K. Satake (2001a), Coseismic slip distribution of the 1946 Nankai earthquake and aseismic slips caused by the earthquake, *Earth Planets Space*, *53*, 235–241.

Tanioka, Y., and K. Satake (2001b), Detailed coseismic slip distribution of the 1944 Tonankai earthquake estimated from tsunami waveforms, *Geophys. Res. Lett.*, *28*(6), 1075–1078, doi:10.1029/2000GL012284.

Thatcher, W. (1984), The earthquake deformation cycle at the Nankai trough, southwest Japan, *J. Geophys. Res.*, *89*(B5), 3087–3101, doi:10.1029/JB089iB05p03087.

Tinti, E., P. Spudich, and M. Cocco (2005), Earthquake fracture energy inferred from kinematic rupture models on extended faults, *J. Geophys. Res.*, *110*, B12303, doi:10.1029/2005JB003644.

Usami, T. (1987), *Descriptive Catalogue of Disaster Earthquake in Japan* (in Japanese), New Edition, 435 pp., Univ. of Tokyo Press, Tokyo.

Victor, P., M. Sobiesiak, J. Glodny, S. N. Nielsen, and O. Oncken (2011), Long-term persistence of subduction earthquake segment boundaries: Evidence from Mejillones Peninsula, northern Chile, *J. Geophys. Res.*, *116*, B02402, doi:10.1029/2010JB007771.

Wells, R. E., R. J. Blakely, Y. Sugiyama, D. W. Scholl, and P. A. Dinterman (2003), Basin-centered asperities in great subduction zone earthquakes: A link between slip, subsidence, and subduction erosion?, *J. Geophys. Res.*, *108*(B10), 2507, doi:10.1029/2002JB002072.

Yabuki, T., and M. Matsu'ura (1992), Geodetic data inversion using a Bayesian information criterion for spatial distribution of fault slip, *Geophys. J. Int.*, *109*(2), 363–375, doi:10.1111/j.1365-246X.1992.tb00102.x.

Yagi, Y., and M. Kikuchi (2003), Partitioning between seismogenic and aseismic slip as highlighted from slow slip events in Hyuga-nada, Japan, *Geophys. Res. Lett.*, *30*(2), 1087, doi:10.1029/2002GL015664.

Yoshida, S., and N. Kato (2011), Pore pressure distribution along plate interface that causes a shallow asperity of the 2011 great Tohoku-oki earthquake, *Geophys. Res. Lett.*, *38*, L00G13, doi:10.1029/2011GL048902.

Yoshioka, S. (2007), Difference in the maximum magnitude of interplate earthquakes off Shikoku and in the Hyuganada region, southwest Japan, inferred from the temperature distribution obtained from numerical modeling—The proposed Hyuganada triangle, *Earth Planet. Sci. Lett.*, *263*(3–4), 309–322, doi:10.1016/j.epsl.2007.08.025.

E. Fukuyama and S. Hok, National Research Institute for Earth Science and Disaster Prevention, 3-1, Tennodai, Tsukuba, Ibaraki 305-0006, Japan. (fuku@bosai.go.jp)

C. Hashimoto, Graduate School of Environmental Studies, Nagoya University, Furo-cho, Chikusa-ku, Nagoya 464-8601, Japan. (hashi@seis.nagoya-u.ac.jp)